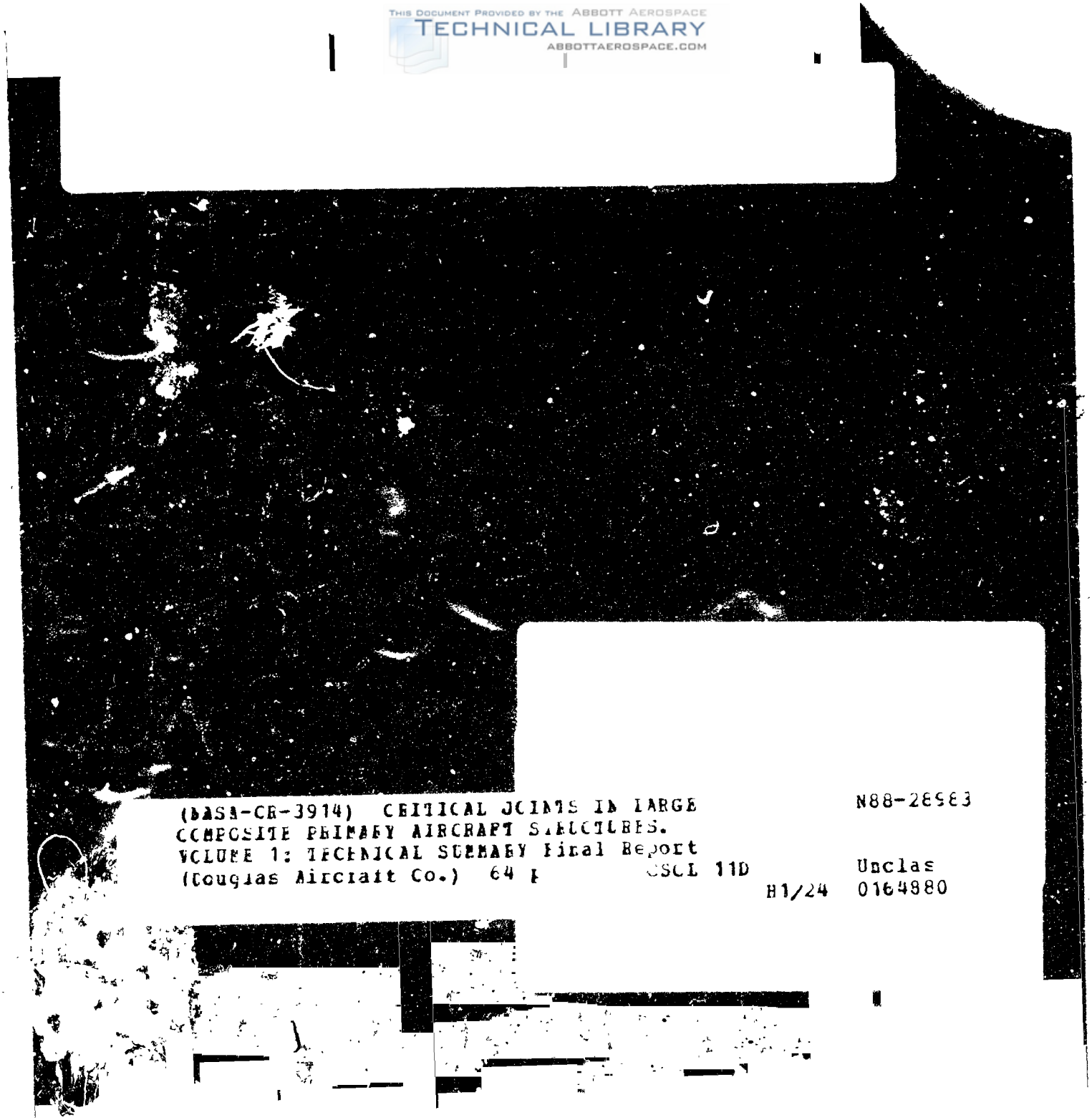

(NASA-CR-3914) CRITICAL JOINTS IN LARGE COMPOSITE PRIMARY AIRCRAFT STRUCTURES. VOLUME 1: TECHNICAL SUMMARY Final Report (Douglas Aircraft Co.) 64 p CSCL 11D

N88-28583

Unclas
H1/24 0164880

NASA Contractor Report 3914

Critical Joints in Large Composite Primary Aircraft Structures

Volume I—Technical Summary

B. L. Bunin

Douglas Aircraft Company
Long Beach, California

Prepared for
Langley Research Center
under Contract NAS1-16857

National Aeronautics
and Space Administration

**Scientific and Technical
Information Branch**

1985

PREFACE

This report — Critical Joints in Large Composite Primary Aircraft Structures, — was prepared by Douglas Aircraft Company, McDonnell Douglas Corporation, under contract NAS1-16857. The project was conducted as part of the NASA Aircraft Energy Efficiency (ACEE) program.

The research effort was monitored by Andrew J. Chapman, ACEE Composites Project Office, Langley Research Center, NASA. Bruce L. Bunin was the Douglas Project Manager. Max Klotzsche was Douglas ACEE Program Manager.

In addition to the author, Douglas personnel contributing to this program included D. J. Watts and W. D. Nelson, prior Project Managers; L. J. Hart-Smith and J. B. Black, Stress Analysis; L. P. Marius, Design; J. V. Walker and E. P. Moenning, Materials; G. C. Janicki and P. J. Marra, Manufacturing R&D, and R. L. Oswald, Program Administration.

CONTENTS

ILLUSTRATIONS

PRECEDING PAGE BLANK NOT FILMED

ILLUSTRATIONS
(Continued)

TABLES

SUMMARY

A program was conducted to develop and demonstrate the technology for critical structural joints of a composite wing structure that meets all the design requirements of a 1990 commercial transport aircraft.

The program was divided into two phases. During Phase I, completed in September of 1983, the procedures for bolted composite joint design and analysis were developed. Tests were conducted at the element level to supply the empirical data required for methods development (Reference 1). Large composite multirow bolted joints were tested to verify the selected design concepts and for correlation with analysis predictions (Reference 2). The Phase I summary is reported in Reference 3. The Phase II program included additional tests to provide joint design and analysis data, and culminated with several technology demonstration tests of a major joint area representative of a commercial transport wing.

SECTION 1
INTRODUCTION

The major objective of this investigation was to develop and demonstrate the technology for critical structural joints of a composite wing structure that meets all the design requirements of a 1990 commercial transport aircraft.

To fulfill this objective, procedures for the design and analysis of bolted joints in composite structures were developed. Structural tests of single-bolt joints were conducted to provide empirical data in support of the design and analysis of multirow joints (Reference 1). Multirow joint specimens referred to as "joint subcomponents" were tested in both tension and compression during the Phase I effort to provide data for correlation with analytical predictions (Reference 2). In most cases, excellent correlation between analysis and test results was demonstrated, verifying the basic analytical approach. The A4EJ computer analysis program was used to design and predict the strength of large multirow bolted joints which usually failed at gross-section strain levels on the order of 0.005. For the material systems and fiber patterns tested, this corresponds to far-field stress levels of roughly 45,000 to 47,000 psi.

The specific objective for Phase II of the program was to demonstrate the technology developed during Phase I with structural tests of representative wing joint structure and to correlate these results with analytical predictions. The critical wing joint selected for the technology demonstration effort was the side of the fuselage splice at the lower rear spar. The test program examined portions of this area separately and culminated in the testing of a large bolted joint specimen representing the aforementioned wing splice which included the wing skin, spar cap, and spar web members. Further development of the analysis methodology was required to properly model the behavior of representative wing joint structure, typically more complex than the relatively simple skin splices tested in Phase I. Semiempirical methods were combined with finite element analysis models and accurate strength predictions were again achieved.

The work was conducted at the Douglas Aircraft Company, Long Beach, California, under contract to NASA-Langley Research Center. The research work performed on this program was based initially on an earlier contract with NASA-Langley on small bolted coupon tests in which the failure mechanisms and strengths for composite laminates with bolt holes were characterized empirically (Reference 3). In a later contract with the U.S. Air Force Flight Dynamics Laboratory at Wright-Patterson AFB, Ohio, the A4EJ computer analysis program was developed for the analysis of multirow bolted joints (Reference 4). Other related work will be discussed throughout the report.

After a review of the Phase I effort, this report will focus on the technology demonstration program of Phase II. The analysis methodology development, structural test program, and correlation between test results and analytical strength predictions are reviewed.

SECTION 2
PHASE I TECHNOLOGY DEVELOPMENT

The Phase I program began with the preliminary design of a composite wing, for a "high-technology" commercial transport aircraft. The baseline aircraft for this effort is shown in Figure 1. The design effort was conducted to the extent required for the conceptual design of critical joints in selected locations throughout the wing structure. An internal loads analysis was performed to establish ultimate load intensities. The outer wing concept was to be manufactured in two segments, with a major joint occurring at the side of the fuselage to a center wing section as shown in Figure 2. The results of the internal loads solution were used along with wing stiffness requirements to design and optimize the skin-stringer spacing and thicknesses based on 37.5-percent 0-degree, 50-percent ±45-degree, and 12.5-percent 90-degree laminate fiber patterns. The material system used throughout the program was Ciba-Geigy 914/Toray T300, primarily in 10-mil tape form. The results of the conceptual design effort are reviewed in Reference 5.

Concurrent with the preliminary design effort, analytical methods were developed for composite multirow bolted joints. In order to achieve accurate strength predictions for multirow joints, the selected analytical approach must begin with a load-sharing analysis that can solve for the bearing and bypass loads at each fastener location. Such a solution must include the nonlinear effects associated with inelastic deformations of the fasteners or joint members. Once the joint load distributions are established, a method is needed for predicting the strength at each fastener hole when subjected to any combination of bearing and bypass loads.

Numerous investigators have examined the problem of estimating stress-concentration factors for composite laminates with fastener holes, the behavior of which, as shown in Figure 3, lies roughly halfway between analytical predictions based on purely elastic and fully plastic behavior. Neither approach comes close to predicting the strength of single-bolt composite joints without some sort of modification, usually consisting of an empirically based correlation factor. The estimation of this apparent nonlinear behavior in the vicinity of a bolt hole can be achieved with the BJSFM method (Reference 6) by comparing the laminate stresses with elastic failure criteria at a "characteristic dimension" from the edge of the hole. In the case of the A4EJ program, the correlation is achieved by modifying the theoretical elastic stress concentration factor at each bolt hole (Reference 7). The stress concentration factor is reduced, on the basis of test results, to account for progressive failure mechanisms including fiber-resin pullout, delamination, and fiber failure. A linear relationship is postulated between the calculated elastic stress concentration factors and the observed factors at failure for the composite material (see Figure 4).

A total of 180 single-bolt coupon tests were conducted in Phase I covering loaded and unloaded holes, tensile and compressive loading, and three bolt sizes — 1/4 inch, 1/2 inch, and 3/4 inch. Most of the specimens were loaded in double shear, but there were a sufficient number of single shear tests to identify any differences in behavior. These tests measured net-section strengths which correspond to the observed stress concentration factors of Figure 4.

Bearing strengths were measured along with the net-section strengths to provide the intercepts of the bearing-bypass interaction curves, which serve as the failure criteria for multirow joint analyses. Other strength limitations such as fastener shear and gross-section allowables are also included. These curves, as shown in Figure 5, are constructed for either tension or compression loads for each fastener hole in each joint member. As the A4EJ program runs through its iterative solution, the bearing-bypass curves are continuously checked until the strength limits are exceeded at one of the fastener holes.

In order to perform the load-sharing analyses, the load-deflection properties at each fastener location must be determined and input to the program as a stiffness property. The single-bolt test specimens were instrumented so that load deflection curves to failure were generated for each configuration, characterizing both the linear and nonlinear ranges of behavior. The load-deflection properties are idealized in the A4EJ program with a simple bilinear model, as shown in Figure 6, in which the second portion of the curve represents plastic deformation. This nonlinear range of behavior can be essential to performing accurate strength predictions, particularly for joint geometries which produce a substantial amount of plastic deformation prior to failure. During the Phase I investigation, it was found that the linear portions of these curves could be represented accurately by minor modifications to an old NACA formula (Reference 8) developed during an investigation of metallic joints.

Having generated the mechanical properties required for the analysis of multirow joints, parametric studies were conducted to evaluate the effects of varying joint proportions and configurations on bolt load distributions and overall performance. The results of one such study are presented in Figure 7, where the effects of varying joint member thicknesses on the fastener load sharing and ultimate joint strengths were evaluated. This study revealed that by tailoring the joint geometry, a bolt load distribution could be generated which maintains a low-bearing high-bypass condition at the first or outermost row of fasteners.

The nature of composite materials is such that the bypass strength is always substantially greater than the bearing strength for reasonably isotropic laminates with bolt holes. Thus, it was determined that the maximum strength for a multirow bolted joint is achieved by minimizing the load transfer at the first row of fasteners where the bypass load is the highest, while allowing the other fasteners to carry the remaining load without permitting a premature failure in some other location. This principle is illustrated in Figure 8 in which typical interaction curves are drawn in terms of loads and stresses.

The methods and data described above were used to analytically predict the strength of 20 large multirow bolted joints tested in the Phase I program. In most cases, good correlation was demonstrated between analysis and test results. Figure 9 shows one of the subcomponent specimens after testing. This particular specimen had a 1-inch-thick center skin and was fastened together with two rows and three columns of 3/4-inch-diameter bolts. The analysis-test correlation for this specimen configuration loaded in both tension and compression is shown in Figure 10 in terms of the associated bearing-bypass interaction curves. The proximity of the predicted and tested strengths shows good correlation in all cases.

The prime conclusion drawn from the Phase I effort was that it is possible to make reliable strength predictions for large multirow bolted joints in fibrous composite laminates. Not all geometries and load conditions were covered, and several aspects of the analysis methodology warrant further development. Nevertheless, the key ingredients in efficient joint design were identified and verified by test. The stress and strain levels achieved at failure for the multirow joints tested were a considerable improvement over the state of the art, and the methodology was developed to the extent that a second phase of the effort was planned to demonstrate the level of technology using large multirow joints representative of actual transport wing structure.

The Phase I program is summarized in Reference 5.

ORIGINAL PAGE IS
OF POOR QUALITY

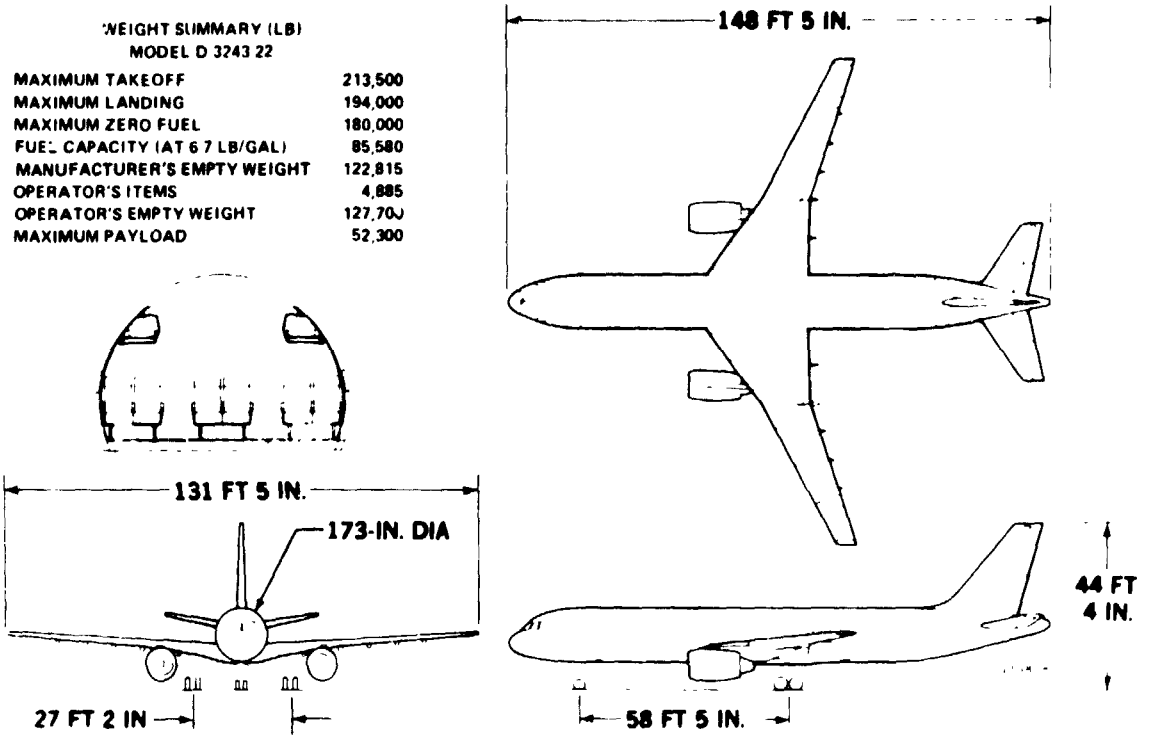

FIGURE 1. BASELINE AIRCRAFT CONFIGURATION

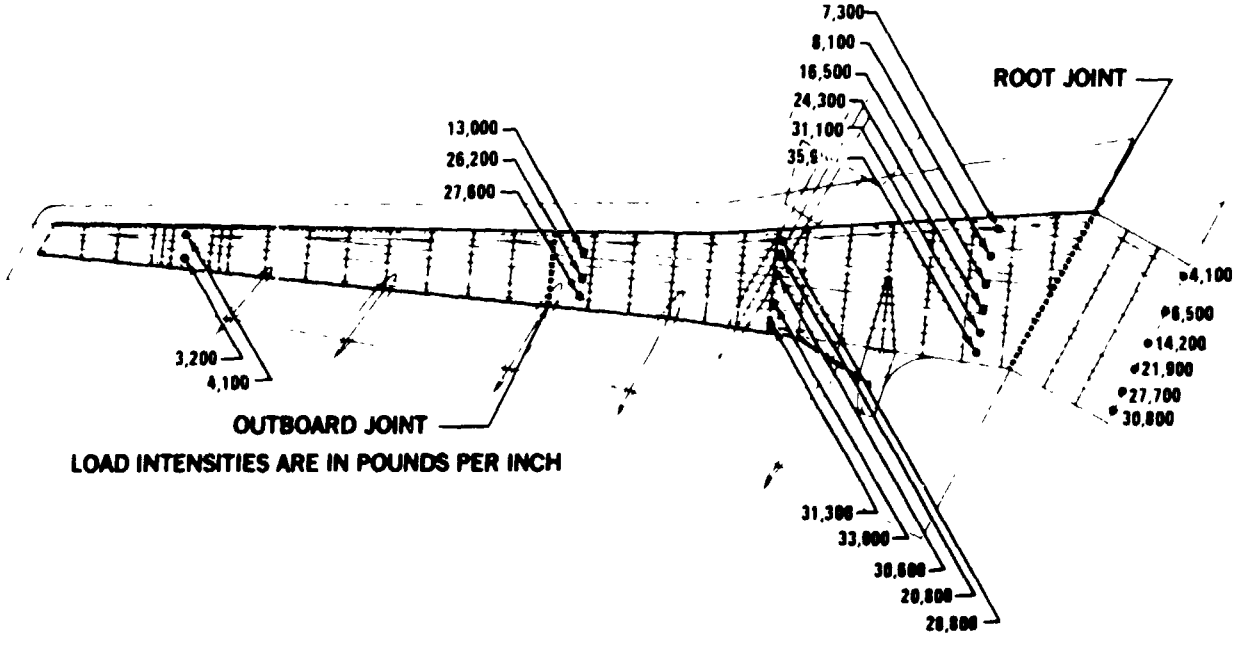

FIGURE 2. WING LOAD INTENSITIES AND JOINT LOCATIONS

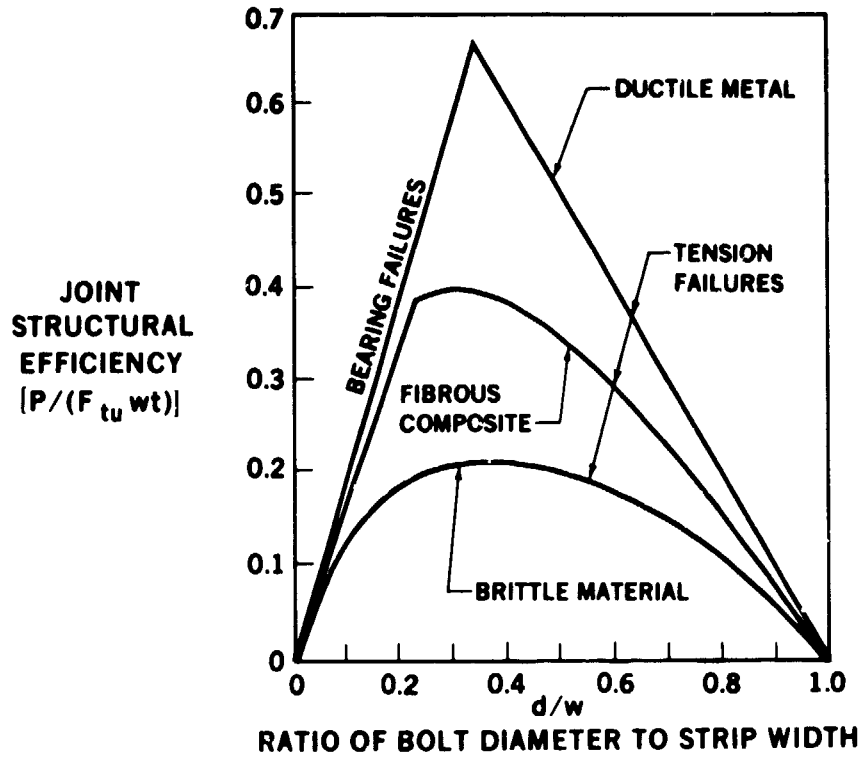

FIGURE 3. RELATION BETWEEN STRENGTHS OF BOLTED JOINTS IN DUCTILE, FIBROUS COMPOSITE AND BRITTLE MATERIALS

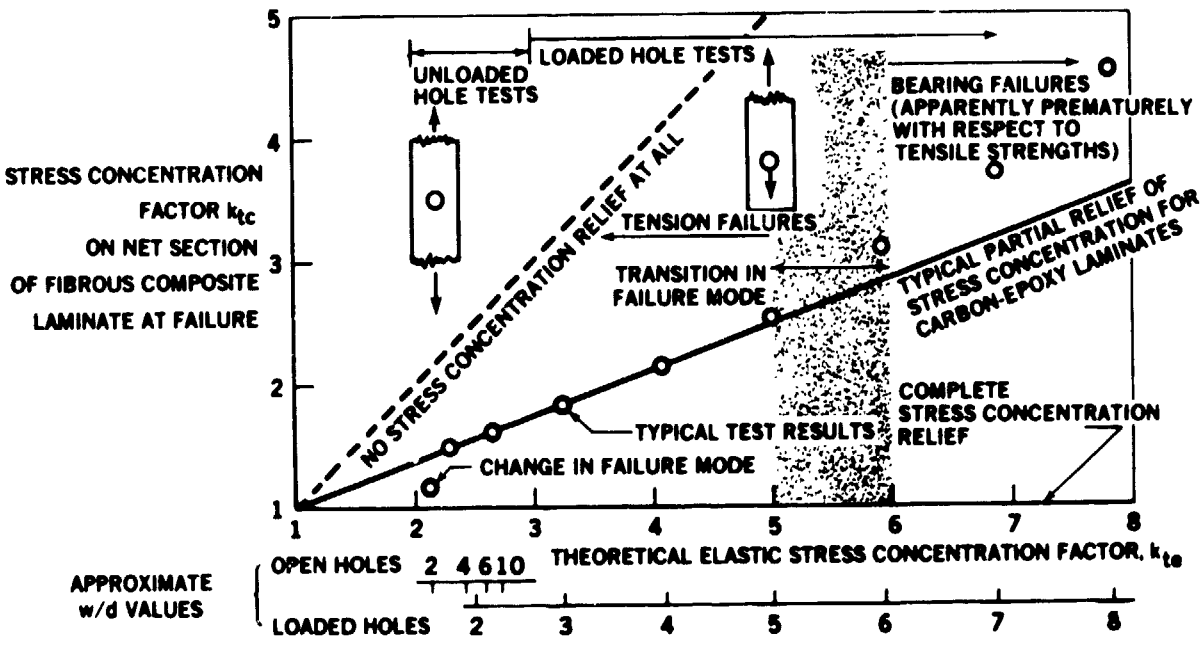

FIGURE 4. COMPOSITE STRESS CONCENTRATION FACTORS

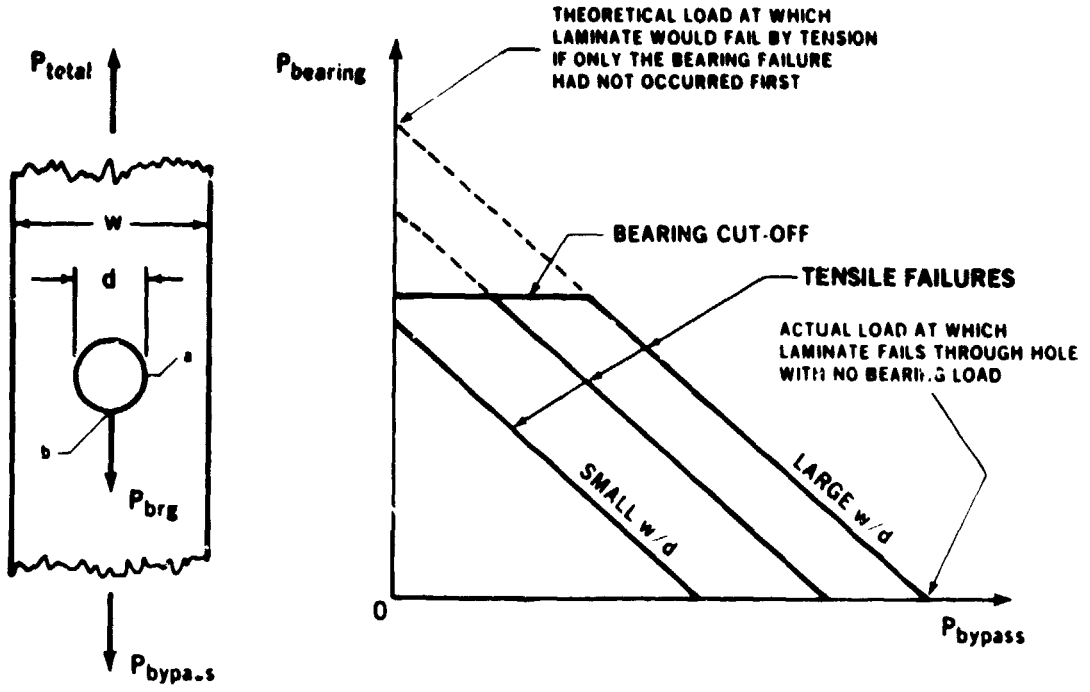

FIGURE 5(a). BEARING-BYPASS INTERACTIONS UNDER TENSION LOAD

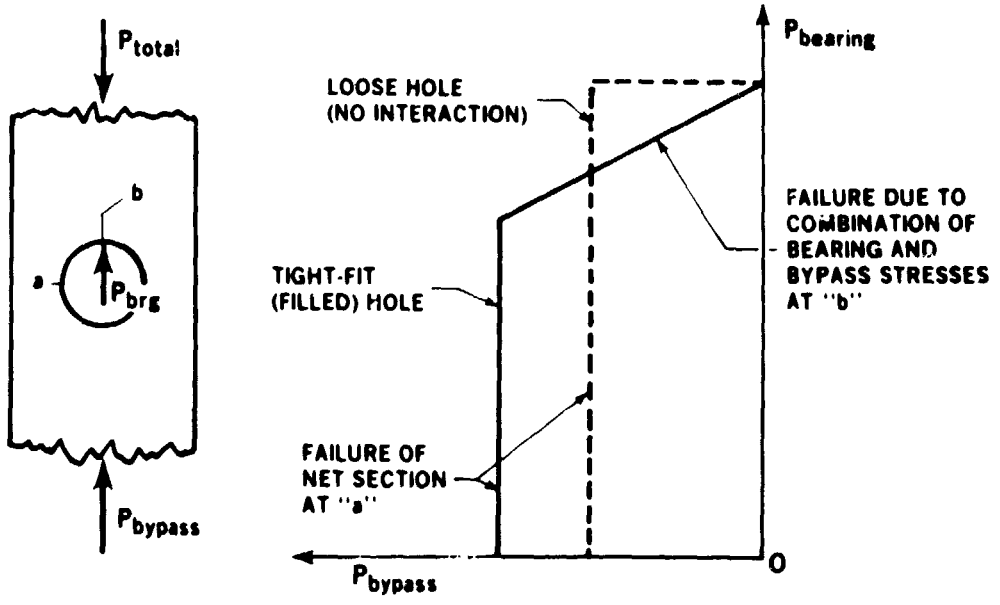

FIGURE 5(b). BEARING-BYPASS INTERACTIONS UNDER COMPRESSION LOAD

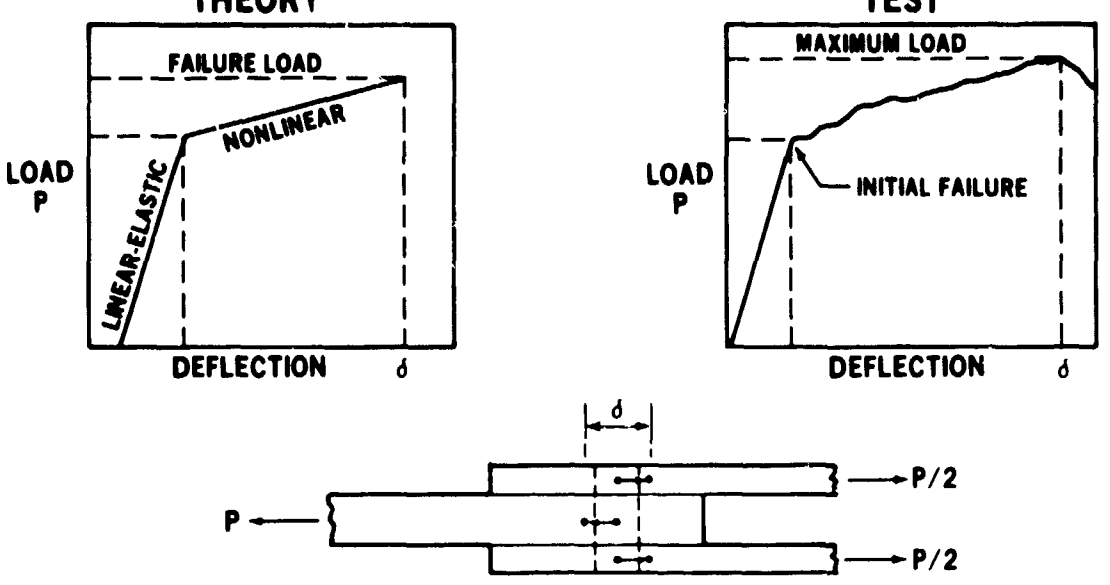

FIGURE 6. FASTENER LOAD-DEFLECTION PROPERTIF

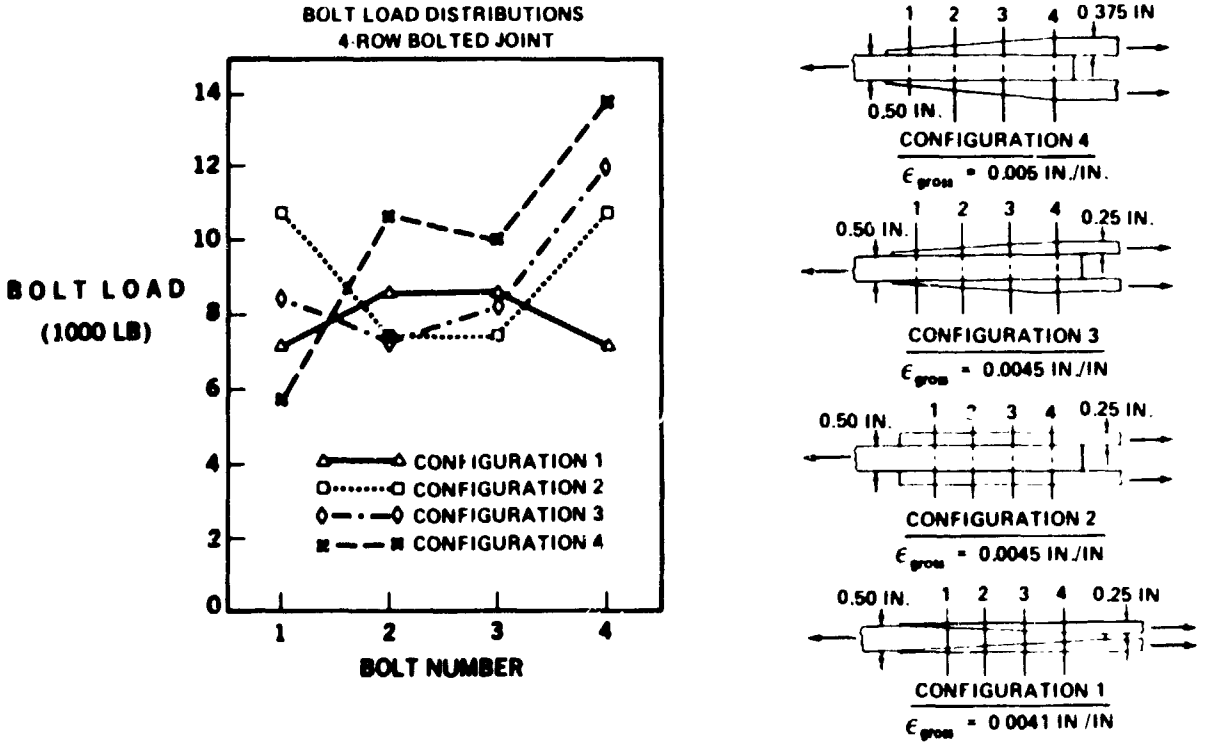

FIGURE 7. EFFECT OF JOINT CONFIGURATION ON BOLT LOAD DISTRIBUTION

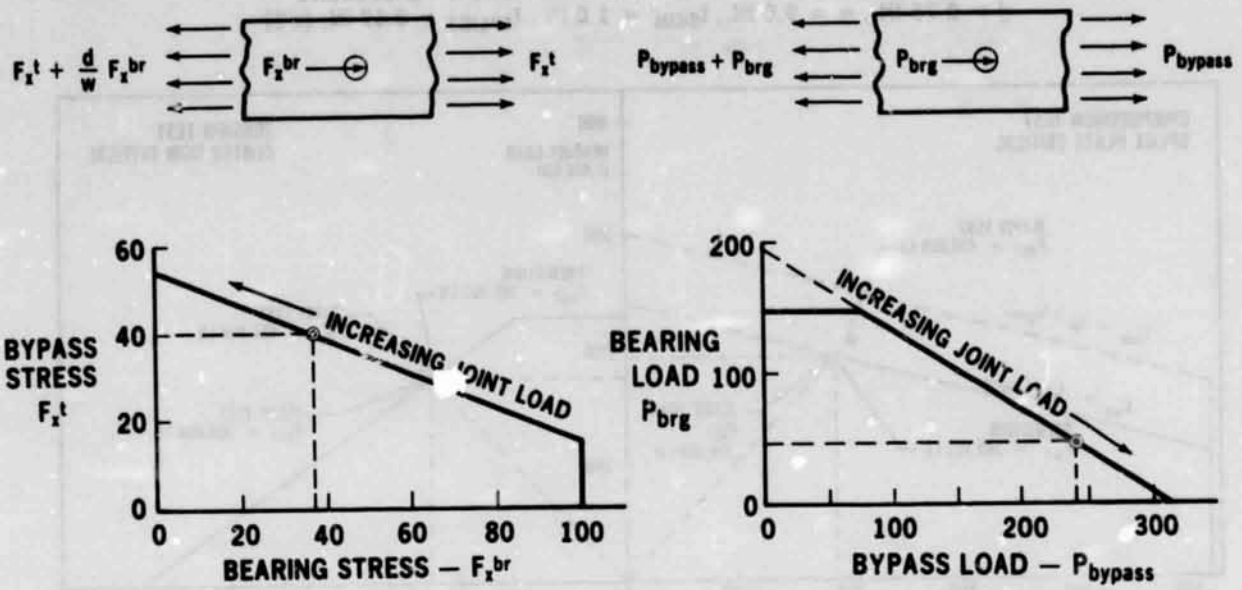

FIGURE 8. BEARING-BYPASS INTERACTIONS MINIMUM INITIAL LOAD TRANSFER APPROACH

FIGURE 9. TWO-ROW, THREE-COLUMN SUBCOMPONENT JOINT, NET-TENSION FAILURE

2-ROW, 3-COLUMN TENSION AND COMPRESSION SPECIMENS
d = 0.75 IN., w = 9.0 IN., t_{SKIN} = 1.0 IN., t_{SPLICE} = 0.67 IN. (x 2)

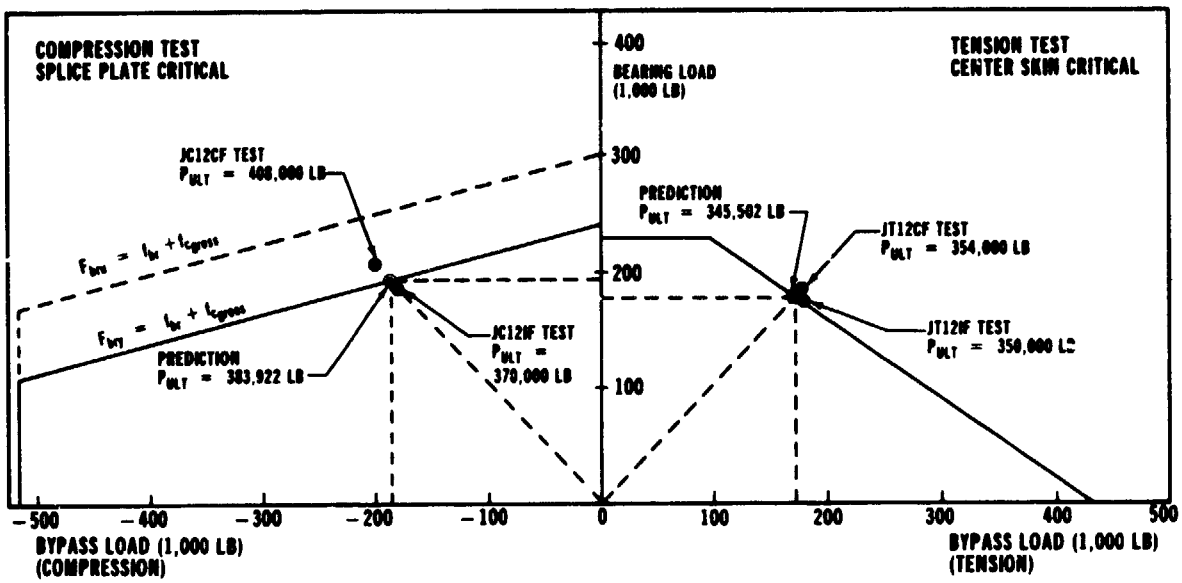

FIGURE 10. BEARING-BYPASS FAILURE ENVELOPES

SECTION 3
CONCEPT SELECTION

Several design concepts were developed during the Phase I program for critical joint locations throughout the wing. Based on the scope and the overall objectives of the Phase II effort, a specific section of critical wing joint structure was selected for the purposes of a technology demonstration. The internal-loads solution for the baseline wing concept indicated running-load intensities of roughly 36,000 pounds per inch near the wing root at the rear spar (Figure 2). Since these load levels were the highest throughout the wing, this portion of the structure was selected for the technology demonstration program.

Critical-joint concepts were developed for the upper and lower cover panels based on the 37.5-percent 0-degree laminate pattern, with gross-section strain levels restricted to 0.0032 to 0.004, depending on the fastener sizes. After ancillary test data became available, a series of A4EJ analysis solutions indicated that strain levels on the order of 0.004 to 0.005 were achievable through careful tailoring of joint proportions to optimize the bolt load distributions. The high-tension load on the wing lower surface was determined to be the most critical condition. Thus, the wing root splice at the lower rear spar was chosen as the basis for the Phase II program.

The design objective for the wing-root splice was to provide a bolted joint of sufficient structural integrity while minimizing the complexity of fabrication and assembly procedures. The original concept shown in Figure 11 includes the rear spar web and the first stringer runout. A portion of the spar cap channel section is shown in a double shear splice along with the wing skin. The stringer runout is accomplished by scarfing off the stringer blade while simultaneously increasing in thickness before entering the bolted joint. The upper surface of the skin and cap members are joined by a titanium "tee" splice plate forming an attach point to the side of the fuselage bulkhead. The lower surface is spliced by an external titanium plate. The spar web and the standing leg of the spar cap are also spliced by a titanium tee on the external surface, and are joined internally by an aluminum corner fitting which transfers load through the side of the fuselage bulkhead with large tension fasteners. The corner fitting is also attached through the skin and spar cap splice, providing additional rigidity to the corner attachment.

Metal materials were selected for the splice plate members for several reasons. Optimum b. load distributions are obtained by tailoring the joint proportions, which includes tapering the splice plates in order to minimize the load transfer at the first row of bolts. During the Phase I program, several of the subcomponent tension joints with tapered composite splice plates suffered premature failures due to unexpectedly high peel stresses and interlaminar forces, as illustrated in Figure 12. Although improved design concepts for these members have been developed, the use of metallic splice plates seemed the most simple and cost effective way of avoiding these potential failure modes. Further, the use of protruding head fasteners on tapered members requires either spotfacing of the splice plate surface or the use of tapered washers under the fastener heads and nuts. Spotfacing into tapered composite laminates introduces potentially critical peel forces in combination with local stress concentration effects, and the use of tapered washers increases the cost and complexity of the assembly procedures. Thus, the use of metallic splice plates with spotfacing on tapered surfaces to accommodate fastener seating was adopted as a standard practice.

Beyond the reasoning discussed above, composite materials are not well-suited to applications where high out-of-plane forces are present. The tee-splice members in the joint concept of Figure 11 are likely to encounter such forces, the magnitude of which are very difficult to predict analytically or measure experimentally. The fabrication of the corner fittings using composite materials would be impractical for similar reasons as well as cost-prohibitive compared to the use of aluminum parts. While the splice plates may be slightly heavier due to the use of metal materials in these applications, any small extra weight in the splices (or fasteners) is worth incurring to maximize the efficiency of the large heavy skins. For a large transport, the weight of the splicing elements as a percentage of the total wing weight is small, and splice efficiencies should not be evaluated solely on the basis of minimum splice plate and fastener weight.

As a basic design philosophy, skin reinforcements or "pad-ups" were avoided wherever possible from the standpoint of both cost and basic skin repairability. A skin pad-up in a bolted splice area where the joint is working to its maximum efficiency implies that bolted joints or bolted repairs in a region outside the pad-up would not be capable of restoring the ultimate strength of the structure. Thus, pad-ups are allowed if warranted by other design considerations, but the joint itself must not be loaded to the point that the surrounding structure would be unrepairable.

Having selected the critical-joint region for this investigation, a test and analysis development program was formulated which would ultimately demonstrate the technology required to design and build critical composite wing joint structure.

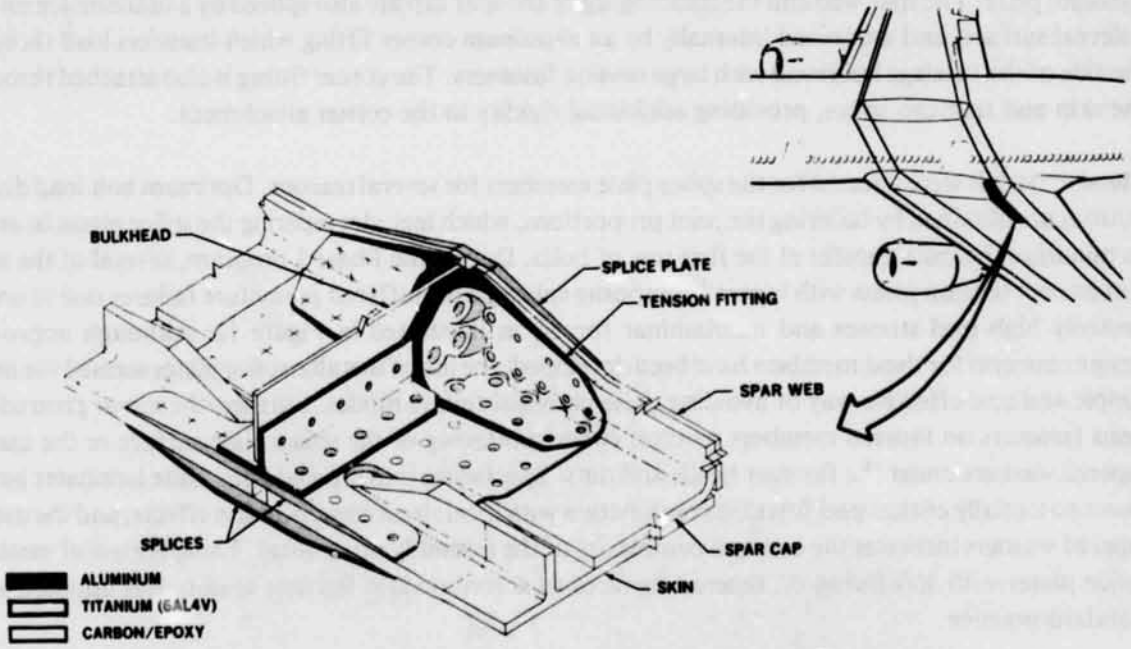

FIGURE 11. LOWER REAR SPAR AND STRINGER CONCEPTUAL JOINT

FIGURE 12. FOUR-ROW TENSION JOINT – SPLICE PLATE DELAMINATIONS

SECTION 4
DESIGN DATA — ANCILLARY TESTS

The Phase II test program began with a series of ancillary tests to further characterize the behavior of single-row composite joints. Tests were conducted for joint geometries which were not tested in Phase I, or where data were inconclusive from previous tests. Unloaded-hole and loaded-hole specimens were tested to determine net-section strengths and the associated stress concentration factors at failure. Wider specimens were tested in the loaded-hole configuration to establish bearing strength limits at the initial point of nonlinearity (bearing yield) and at ultimate load. These tests provide the intercepts for the bearing-bypass interaction curves, serving as the failure criteria for multirow joint analyses. The ancillary test program is reported in Reference 1.

STRENGTH PROPERTIES

Several of the tension coupon specimens tested in Phase I suffered premature failures at the point of load introduction. Thus, a series of unloaded-hole tension specimens were tested in Phase II to recover missing data points and extend the existing data base. The fastener diameters ranged from 0.375 to 1.0 inch, and were tested at width-to-diameter ratios of 3 and 5. Two sets of specimens were fabricated which were identical in every way except for the ply thicknesses — 5-mil tape was used for one set, 10-mil tape for the other. From the results of these tests (Reference 1) there appears to be no significant difference in strength between laminates fabricated with either of the two ply thicknesses. However, a difference in the appearance of the failed specimens was observed, with the 10-mil specimens suffering substantial delaminations around the hole at failure while the 5-mil specimens exhibited a more uniform (clean) net-section failure.

The results of these tests were used to calculate the stress concentration factors at failure of the composite laminates, which are plotted against the calculated elastic-isotropic stress concentration factors in Figure 13. The trends indicated by this plot suggest that the relationship between K_{te} and K_{tc} is not perfectly linear for a line constrained through the point (1,1). Thus, the stress concentration relief factor, referred to as "C" factor, does not appear to remain constant for variations in the specimen width-to-diameter (w/d) ratio. While a complete characterization of this relationship would be useful, the data supplied by this limited series of specimens was sufficient to provide the analytical data base required for the analysis of the multirow joints to be tested in this program. A much more extensive series of tests would be required to fully account for changes in hole size, thickness, w/d ratio, fiber pattern, material system properties, etc.

Loaded-hole tension specimens were tested to provide net-section strengths and laminate bearing strengths. The results of the narrow specimen tests (w/d = 3) which failed in net-tension are also plotted in Figure 13. These results are consistent with the results of Phase I tests, where a value for C of roughly 0.42 was typical of loaded-hole tension failures for the laminate pattern with 37.5 percent 0-degree fibers.

The loaded-hole, double-shear specimens tested during the Phase I program all had external splice plates which were one-half the thickness of the central skin. For the wider specimens designed to measure laminate bearing stress allowables, all failures occurred in the splice plate members at bearing stress levels of around 100 ksi. This failure mode was expected, due to the relatively small amount of clamp-up provided by the fastener heads and nuts, as compared to the clamp-up afforded the center

plate which is sandwiched between the two splice members. This condition is aggravated by bending of the fasteners under load as illustrated in Figure 14. Regardless of whether the applied loads are tensile or compressive, the bolt deflection and rotation are such that the clamp-up on the bearing side of the fastener hole is relieved as the applied load is increased. This lowers the resistance to delaminations of the outer plies under bearing loads and can drastically reduce the allowable bearing stress levels for laminates on the outer surface of composite bolted joints.

In order to obtain realistic bearing stress allowables for the center members in a double shear joint, several coupons were tested in Phase II with composite or metallic splice plates of sufficient thickness to force the failure to occur in the central members. These tests resulted in ultimate bearing stress levels of roughly 160 ksi for the fully clamped central plates, representing a 60-percent increase in strength over that of external composite splice members.

The ancillary test results provided the database required to fully characterize the bearing-bypass interaction curves for typical multirow joint configurations. While all of the large multirow joints tested throughout the program used the (37.5/50/12.5) fiber pattern, single-row joints using quasi-isotropic laminates (25/50/25) were also tested as a baseline. The strength limits of single-row and multirow joints can be plotted in terms of the joint geometry, shown in Figure 15. This plot was constructed for the quasi-isotropic, with the lowest curve representing the maximum strengths that can be achieved with a single-row joint. For this laminate, the maximum strength is reached at a w/d ratio of about 3 to 1, with a structural efficiency (unnotched strength divided by notched strength) of roughly 40 percent. The upper curve in the chart indicates the limiting case of an unloaded hole, while the curves in between represent various combinations of bearing and bypass loads. Thus, it is clear from these plots that the maximum strength for a multirow joint is obtained by minimizing the bearing stress at the critically loaded bolt, where the bypass stress is the highest.

A similar plot is presented in Figure 16 for the orthotropic laminate (37.5/50/12.5) which was selected for the composite wing structure. This chart illustrates that, depending on the geometry, joint strengths roughly 10 to 20 percent greater than that for the quasi-isotropic laminate can be achieved. (It should be noted that these plots were constructed using unnotched strength values about 15 percent lower than the tested values. However, since this was the case for both laminates, the trends indicated by comparison of the two figures are typical.) These results suggest that a tradeoff exists between the added strength due to the increase in 0-degree fibers and the associated increase in stress-concentration factors.

This tradeoff is explained in Figure 17, where the two fiber patterns are compared in terms of the strength and strain levels at failure for a typical multirow joint, as well as the unnotched strengths of the basic laminates. The bearing-bypass curves shown in the lower left-hand corner of Figure 17 represent typical strength envelopes for each of the two fiber patterns. The dashed line follows a path of low bearing and high bypass load, typical of the condition found at the first bolt row of an efficiently designed multirow joint as shown in the sketch to the right.

This chart shows that while the pattern B laminate has a 40-percent greater strength in unnotched tension than the pattern A laminate, the strength increase for a typical multirow joint is only 17 percent due to the higher stress concentration factors for the B pattern. Furthermore, since the relative difference in laminate modulus values is greater than the difference in joint strengths, the strain-to-failure for the pattern A joint is actually 7 percent greater than that for pattern B. Thus, two key points cannot be over-

looked during the design process for composite joints: (1) an increase in unnotched laminate strength does not translate into an equivalent increase in joint strength; and (2) where the laminate fiber pattern is still a design variable, optimizing the joint for maximum strain does not guarantee the highest strength or most weight-efficient design. The principal parameter governing the design of composite bolted joints is the amount of load that must be transferred, not the operating strain level of the adjacent structure.

LOAD-DEFLECTION PROPERTIES

The loaded-hole tests were also used to determine the load-deflection characteristics of single-bolt composite joints. As discussed in Section 2, these properties are required as input data for use in performing the load-sharing analyses for multirow bolted joints. Most of the configurations tested in Phase II were sufficiently different from those of Phase I to provide a valuable addition to the existing database and to further verify the accuracy of the methods developed during Phase I for the prediction of elastic spring rates.

The measured spring rates for the Phase II tests are plotted against the analytically predicted values in Figure 18. The tested values shown are the average results of three identical specimens, while the predicted values were calculated from the aforementioned semiempirical equation developed in Phase I. With the 45-degree line on the plot representing perfect correlation, these results were very encouraging in that good correlation was again demonstrated between predictions and tested values. For those specimens with composite skins and splices (in all but one test series), the variations between the tested averages and predicted values were less than the amount of scatter between test results among the sets of identical specimens.

This was not the case for specimens with composite skins and titanium splice plates for which the tested spring rates were somewhat greater than corresponding predictions. These differences between test and analysis, while not overly significant, should be accounted for in the analysis of multirow joints using similar configurations. To speculate, the higher spring rates may be the result of several phenomena. The titanium joint members maintained a measurably closer hole tolerance or were closer to "net-fit" than similar composite parts. This may have provided a more rigid foundation for the fastener, restricting the elastic bending of the bolt and producing a higher spring rate. It should also be noted that the general trend, as shown in Figure 18, was for the tested spring rates to fall above the predicted values — somewhat in contrast to the Phase I results. The slightly higher stiffnesses for the Phase II tests may have resulted from the higher fastener torque values used in this series which, if nothing else, would increase the friction force between plates and produce a stiffer load path.

Parametric studies were conducted throughout the program to evaluate the effects of variations in joint geometries on the resulting elastic spring rates. Using the equation developed during Phase I, plots were constructed as shown in Figure 19 to analytically predict these effects. In general terms, the elastic spring rates are a function of the joint material properties, the bolt-diameter-to-skin-thickness ratio, and the skin-to-splice-plate-thickness ratio. Where the splices are very thin with respect to the bolt diameter, the stiffness of the load path remains relatively low due to high bearing stresses. When the splice plates become too thick, a drop in the elastic spring rate is predicted because of excessive bolt bending. Maximum stiffness exists somewhere in between these two extremes, as shown in Figure 19, depending on the relative dimensions and sizes of the joint components.

BOLT BENDING

During the Phase I investigation, several single-row and multirow joint specimens suffered "premature" failures due to bending of the fasteners. One such failure is shown in Figure 20, where the severe bolt bending eventually led to failure of the fasteners in combined shear and tension, or to shear failure of the threads between the shear-head nuts and fasteners. In nearly every case, these failures resulted from an overestimation of the fastener strengths, rather than by underestimating the strength of the composite members. Bolt bending failures (defined here as caused by a severe plastic bending of the fasteners) were observed at load levels as low as 50 percent of the rated fastener shear strength. Thus, a routine evaluation of the fastener size solely on the basis of shear strength proved to be inadequate.

The potential for bolt bending failures can often be more significant for highly loaded composite structures than for metallic components. Because of the lower efficiency levels attainable with bolted joints in composites compared with metallic structures (Figure 3), highly loaded composite members can often require more thickness than a metal counterpart for an equal amount of load transfer. As the fastener diameter decreases with respect to the joint member thicknesses (decreasing diameter/thickness, or d/t ratio), the additional eccentricity leads to an increase in fastener bending deflections for a given load level. Furthermore, any increase in elastic bending deflections will contribute to the loss of clamp-up, and lower the effective bearing stress allowables, as discussed earlier in the section on Strength Properties.

Design guidelines for the selection of fastener sizes typically have been based on the fastener shear strength and on some limitation of the allowable d/t ratio. However, such a broad criterion can sometimes be either unconservative or overly conservative, depending on the relative dimensions of the members to be joined and the splicing material through which the load is transferred. The chart shown in Figure 21 was developed in an effort to provide a more comprehensive method of selecting fastener sizes, with consideration given to the bearing strengths of the materials to be joined, the fastener shear strength, and the potential for bolt bending failures. The bolt bending failure curves were derived from limited test results and assume that the bending failures are a function of the d/t ratio for both the skin and splice members (Reference 9).

Figure 21 was developed for double shear joints and is nondimensionalized, except for the center skin bearing stress allowables which are plotted in units of ksi. The chart shows that for low values of d/t_2 (where t_2 is the thickness of one splice plate), a d/t_1 (for the central skin) of roughly 1.0 is near optimum for bearing stress allowables that are typical of composite joints. The bending failure curves show that at low d/t ratios for both the skin and splice plates, bolt bending failures can occur at low percentages of the joint member bearing strengths and fastener shear strengths. As the d/t_2 ratio increases, the propensity for bolt bending failures decreases due to the lower eccentricity, and the fastener shear strength becomes the limiting factor. Eventually, as the d/t_2 ratio become large, the splice plate bearing strengths become the strength cutoff, as indicated by the dashed lines to the upper left in Figure 21. It should be noted that the bolt bending curves on this chart are approximate, and will likely require modification as more test data are obtained. All potential failure modes can be included on this chart except, of course, for net-section failures, which must be calculated separately.

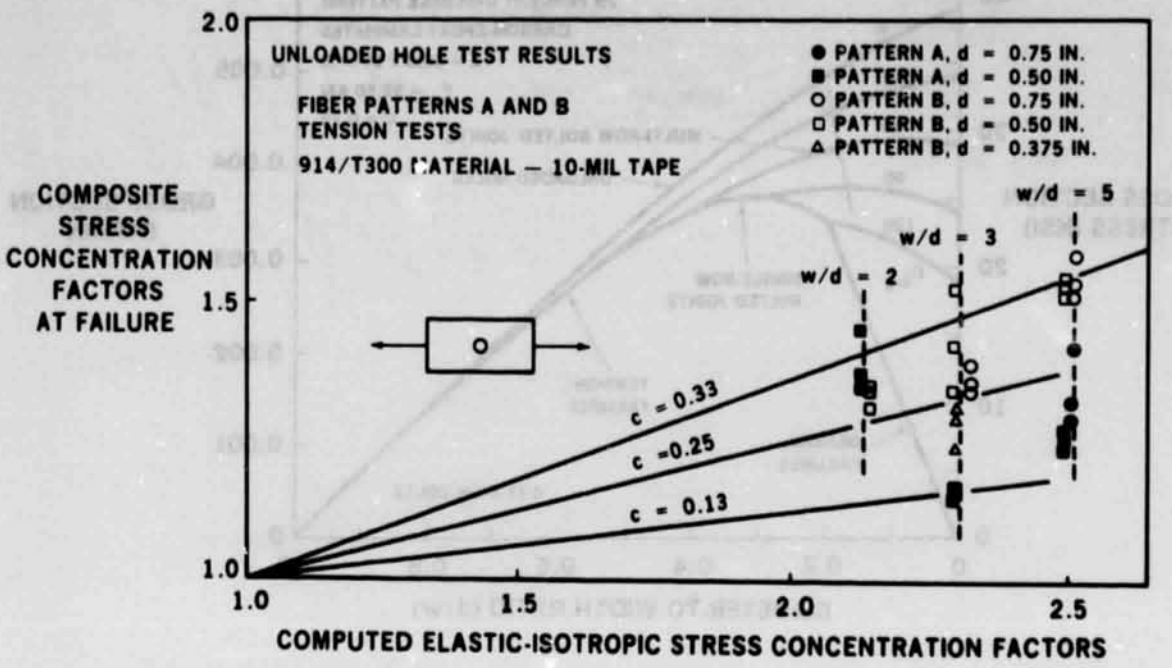

FIGURE 13. COMPOSITE STRESS CONCENTRATION FACTORS AT FAILURE

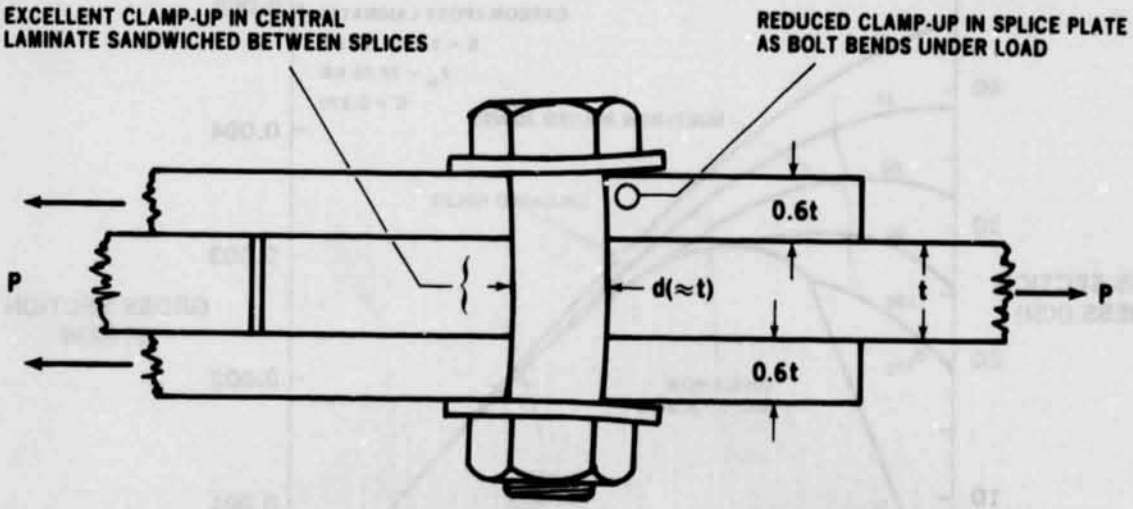

THE BOLT-BENDING EFFECT SHOWN IS ACTUALLY MINIMAL FOR d = t BUT BECOMES PROGRESSIVELY MORE SEVERE FOR SMALLER BOLT DIAMETERS

THE CONSEQUENCE OF THIS EFFECT OF BOLT BENDING IS EVEN MORE PRONOUNCED FOR COMPRESSIVE LOADS

FIGURE 14. BOLT BENDING EFFECTS FOR COMPOSITE JOINTS

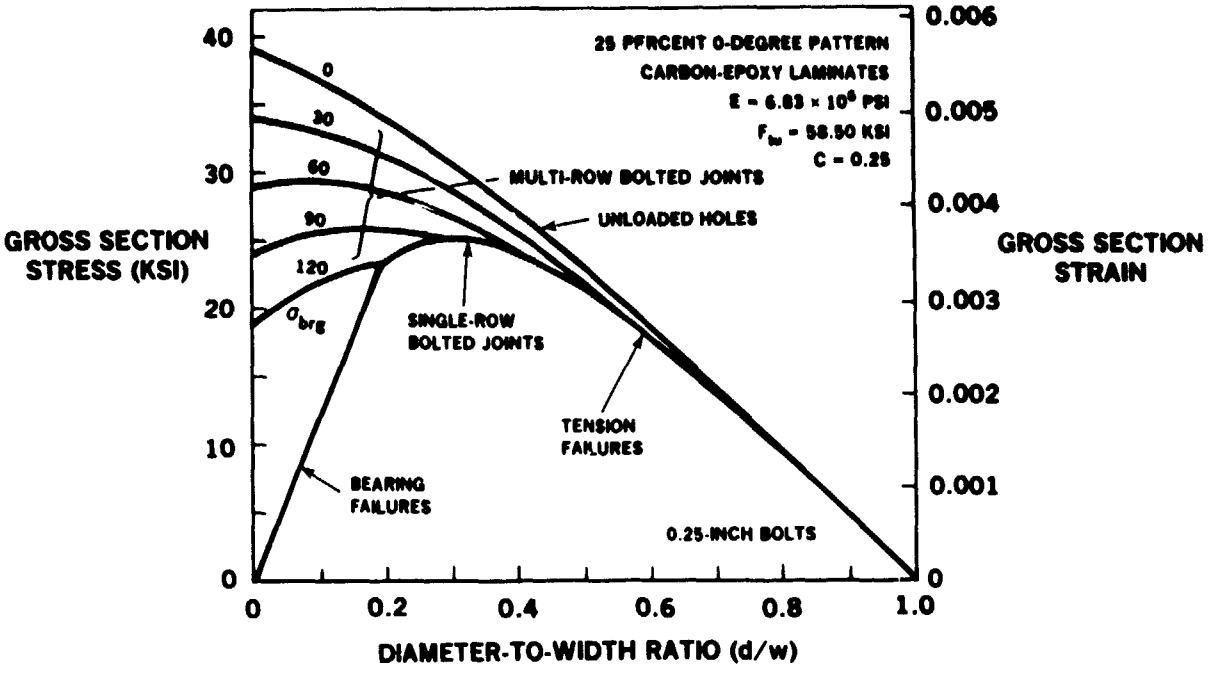

FIGURE 15. BOLTED COMPOSITE JOINT EFFICIENCY CHART (25-PERCENT 0-DEGREE PLIES)

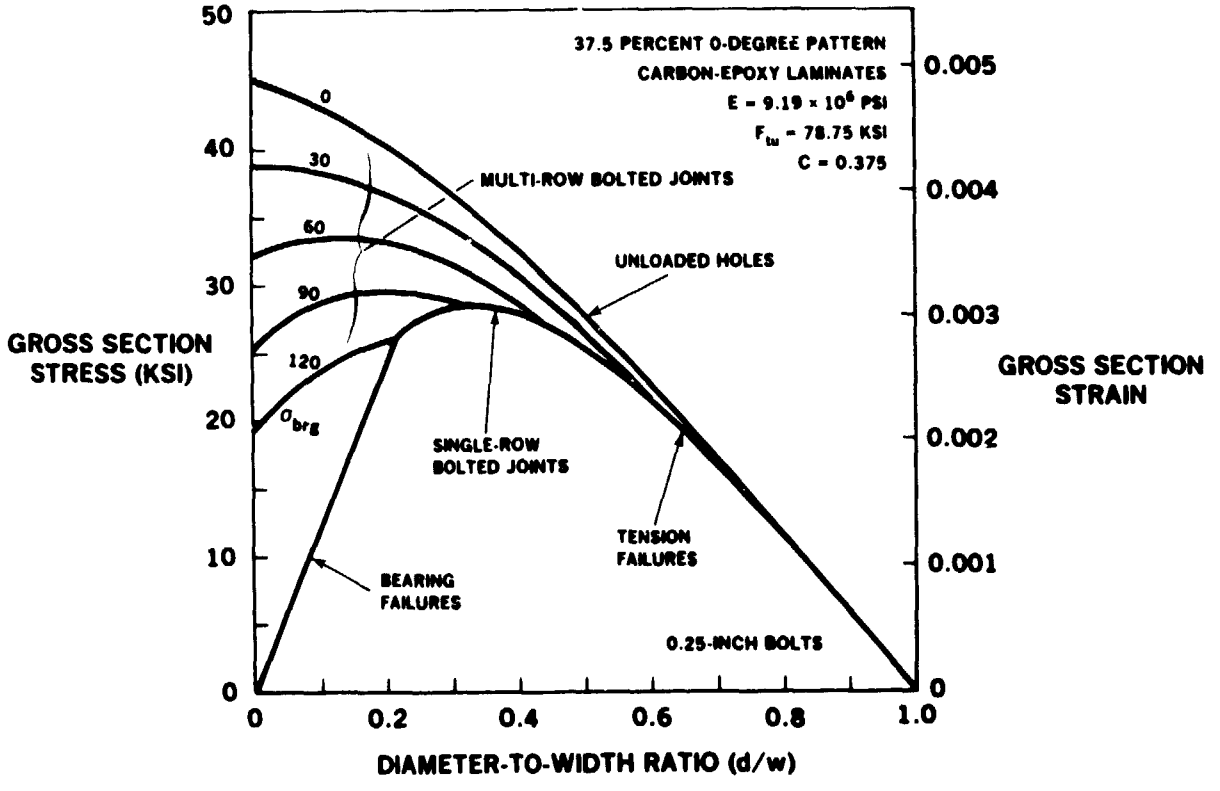

FIGURE 16. BOLTED COMPOSITE JOINT EFFICIENCY CHART (37.5-PERCENT 0-DEGREE PLIES)

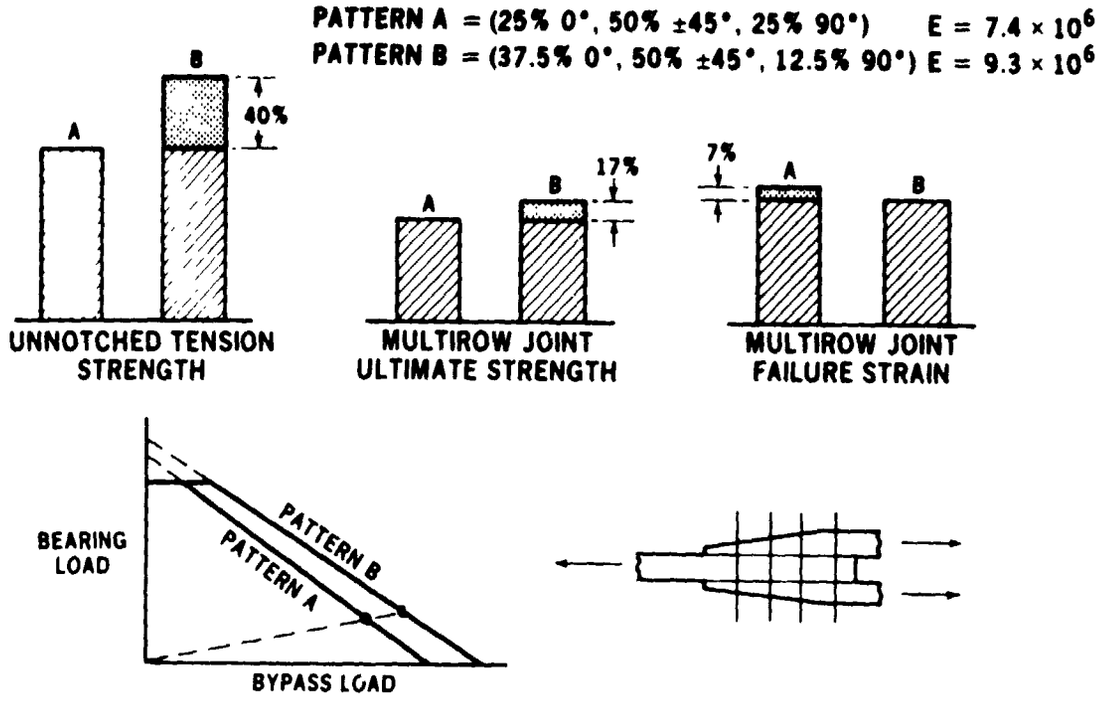

FIGURE 17. EFFECT OF FIBER PATTERN ON MULTIROW JOINT STRENGTH AND STRAIN LEVELS

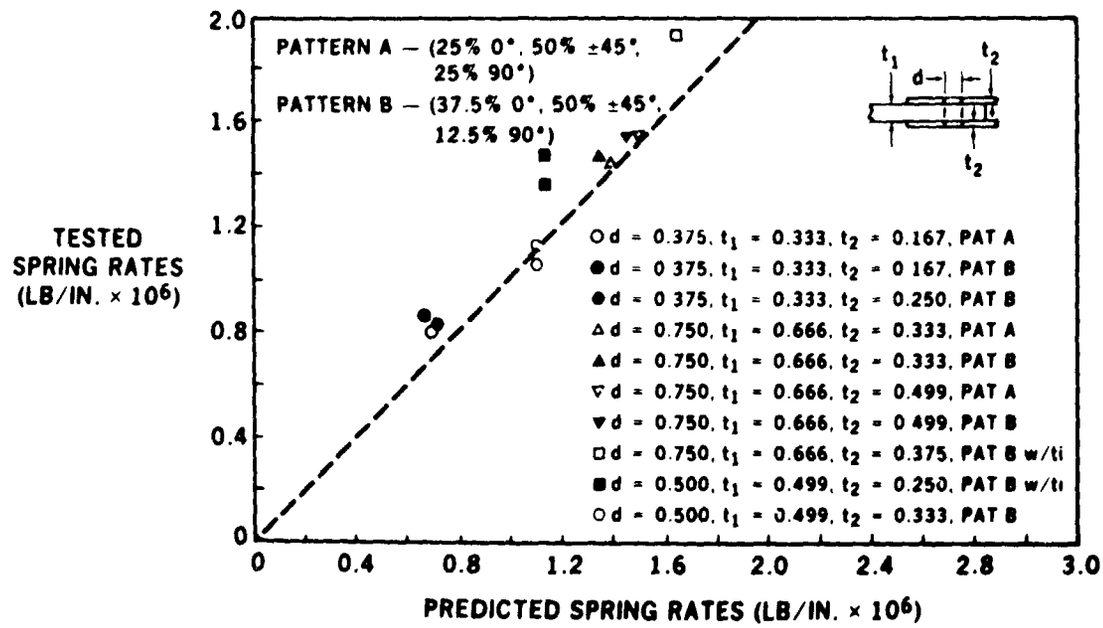

FIGURE 18. BOLTED JOINT ELASTIC SPRING RATES – PHASE II DOUBLE SHEAR TEST VERSUS PREDICTION

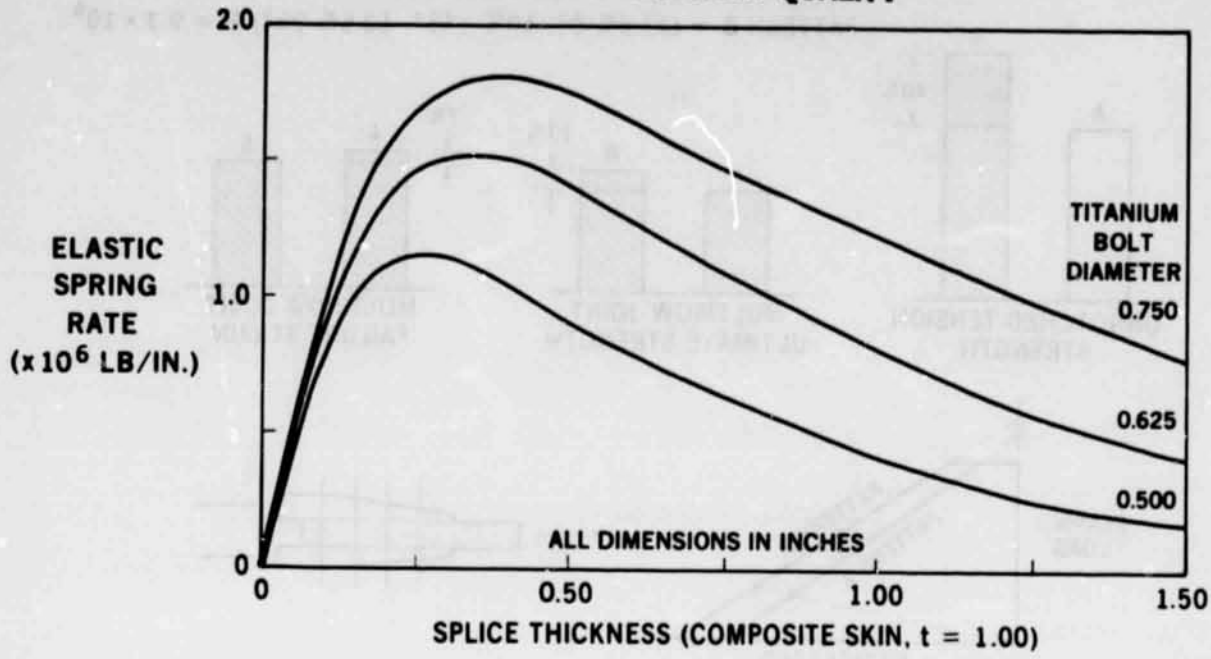

FIGURE 19. PREDICTED ELASTIC SPRING RATE

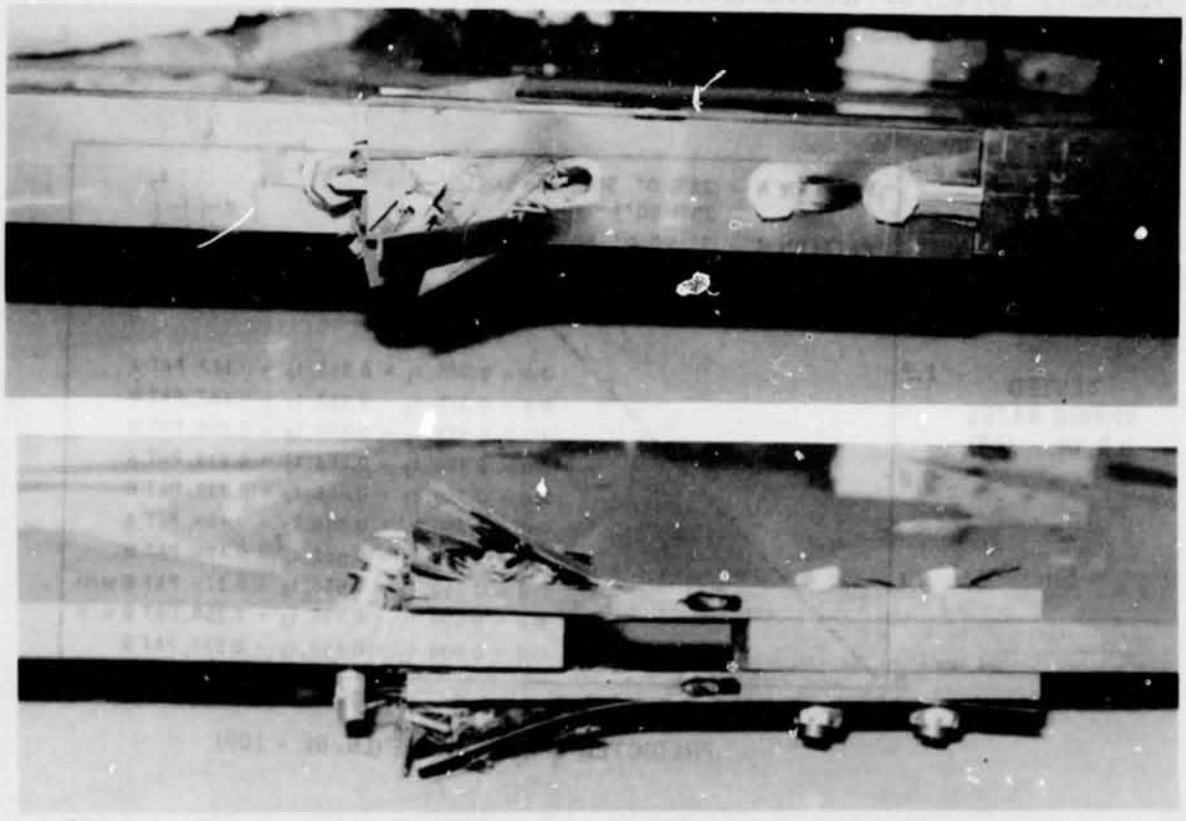

FIGURE 20. TWO-ROW BOLTED JOINT – BOLT FAILURE

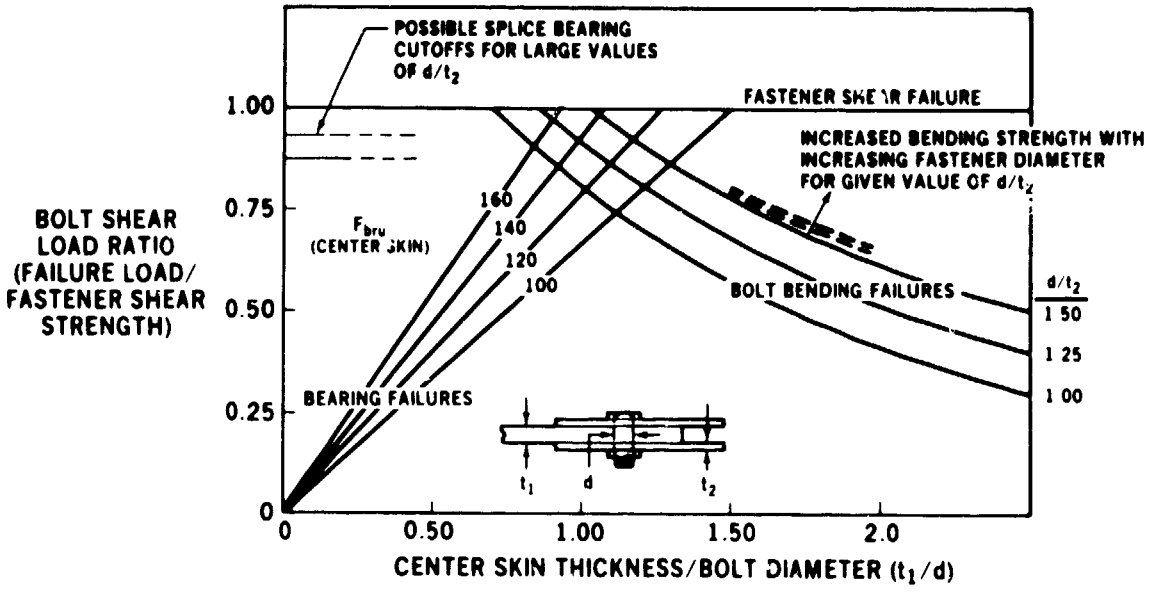

FIGURE 21. APPROXIMATE SINGLE-ROW JOINT ALLOWABLES

SECTION 5
TECHNOLOGY DEMONSTRATION TEST PROGRAM

The Phase II test program concluded with a series of large multirow bolted joint specimens representative of the lower rear spar splice at the side of the fuselage as described in Section 3. Because of the complexity of this portion of the structure, a technology demonstration test program was formulated to investigate portions of this area individually. The test program is described graphically in Figure 22. The stringer transition joint was tested as a separate specimen, while portions of the corner joint representing the skin-spar cap and spar web splices were tested as subcomponents. The test program culminated with the testing of a large bolted joint specimen representing the entire skin and spar corner splice, without including the stringer transition.

This approach to the test program was adopted for several reasons. The greater complexity of representative structure compared with the relatively simple joints tested in Phase I required further development of the analysis methodology. By testing several individual components of the corner joint structure, the accuracy of the selected analytical approach could be evaluated prior to the large technology demonstration test. In addition, the strength of these individual portions of the structure and the efficiency of the chosen design concepts could be measured more directly by these individual tests. This was particularly appropriate for the stringer transition joint test in which the strength of the stringer blade transition was demonstrated to exceed that of the bolted splice. The technology demonstration test was a final verification of the design concepts, manufacturing methods, and analytical approach.

All of the Phase II multirow joint tests were static tension tests. Each specimen was loaded to what was considered a "limit load" level, after which the specimen was inspected visually to ensure that no premature failures or damage had taken place. All of the joint members representing the wing cover panel structure were composite laminates made with the Ciba-Geigy 914/T300 material system in 10-mil tape form. The splice plates for each specimen were metallic, made either of aluminum or titanium. In each case, the laminate fiber pattern was (37.5% 0°, 50% ±45°, 12.5% 90°). All fasteners were made of titanium.

STRINGER TRANSITION TEST

The stringer transition joint was the first of the multirow bolted joints to be tested in Phase II. The concept shown in Figure 23 represents the lower wing skin with an integral blade stringer which transitions into a bolted shear joint at the side of the fuselage. The stringer blade is scarfed along the length of the bolted joint while a thickness buildup is introduced in both the skin and the stringer. The transition is initiated just beyond the first row of fasteners in the skin splice to maximize the bypass load at the critical row of fasteners.

Several design concepts were considered for the stringer joint. The objective was to develop a concept which would be appropriate not only for the side of the fuselage splice but for any portion of the wing structure where a stringer runout or transition is required. Further, the selected concept was to be of minimum complexity from a manufacturing standpoint while maintaining a satisfactory level of structural integrity. After evaluating several candidate design concepts, the scarfed stringer approach was selected. This method eliminates the need for a bolted connection through the stringer blade itself, greatly simplifying the fabrication and assembly requirements.

The primary concern for this design was the strength at the tip of the stringer transition where the high load transfer combined with stress concentration effect could lead to critical out-of-plane forces. To counteract these effects, continuous plies were maintained wherever possible and thickness transitions were achieved with taper angles that were shallow enough to reduce the inherent peel forces below critical levels. The section was laid up with the stringer blade at full depth, and was later machine-tapered.

Tapered titanium splice plates were used to transfer the load into the composite structure. The titanium fasteners varied in diameter from 7/16 inch at the thin end of the splice to 5/8 inch at the thick end. The composite skin and blade sections outside the joint were nominally 0.504 inch and 0.426 inch, respectively. These features were incorporated in the design in an attempt to optimize the bolt load distributions and maximize the strength of the joint. The skin-stringer combination was designed to an ultimate design strain level of roughly 0.005 inch/inch (or 46,500 psi) for the lower wing surface.

The stringer joint specimen is shown in Figure 24 fully assembled and mounted in the test machine. The specimen was fabricated with a stringer transition at each end, and the titanium splice plates were extended to form the points of attachment to the test machine. This greatly simplified the specimen and its assembly by combining the end fitting joints with the test section(s). One end of the specimen was equipped with axial strain gages to monitor joint load distributions throughout the test, while the other end was coated with a photoelastic material.

The photoelastic coating was used to provide a qualitative assessment of the structural response and to identify any unforeseen areas of high stress intensity. It is possible to obtain quite accurate stress-strain measurements using this technique. (Through the use of a polariscope, the fringe orders can be measured to within 0.01 fringes, where each fringe indicates a variation of 10,000 psi. However, this level of accuracy was unnecessary for this specimen since it was possible to mount strain gages at the other [identical] end).

Photographs of the coated regions were taken at several load levels throughout the test. The photograph shown in Figure 25(a) shows the variation in stress for the constant-thickness blade from the skin surface to the top of the section. The change in direction or "bend" in the fringe patterns just outside the bolted joint results from the increase in thickness which occurs simultaneously in the skin and stringer at that point. (The stress level is increasing from the edge of the blade towards the skin.) A slight decrease in stress level is also visible in the blade section along the length of the bolted joint as the load in the composite member is transferred into the splice plates. Strain gages mounted at the other end of the specimen confirm the load distributions as indicated by the photoelastic survey.

The photograph shown in Figure 25(b) illustrates the stress distributions on the surface of the upper titanium splice plate and along the edge of the stringer blade. The tip of the stringer transition had been identified as a potentially critical location, and the photoelastic coating clearly showed the sharp increase in stress level at that point. This view also shows the complex stress field on the surface of the titanium splice member. This condition, resulting from the combination of stress concentrations (due to fastener holes and spotfacing), hole shadowing (regions of low stress between fasteners), and a thickness transition illustrate the difficulty in placing a strain gage on the surface of such a member to monitor the bolt load distributions along a multirow bolted joint.

Though the conclusions that can be drawn from the photoelastic measurements are primarily quantitative, the stress distributions in each member as indicated by the coating provide useful information regarding the specimen structural behavior which can also be used for correlation with analytically predicted trends. A complete set of photographs from this test are presented in Reference 10.

The joint transition specimen was tested to static failure at an ultimate load of 197,200 pounds, or at a running load intensity of about 34,300 pounds per inch. This corresponds to an average gross-section stress and strain level of roughly 50,000 psi and 5,300 microstrain in the basic section, prior to the thickness buildup outside the joint. It should be noted that these "average" values are for the entire cross-section, which is actually varying in stress and strain level from the base of the skin to the top of the stringer blade. Strain gages mounted on the skin outside the build-up indicated a strain level of about 5,900 microstrain, which would correspond to a strain level in the thicker section at the bolted joint of roughly 4,700 microstrain. The Young's modulus for the test laminate was 9.3×10^6 psi.

The specimen failed in net-section tension through the first (outermost) row of fasteners at a high-bypass, low-bearing load combination, followed by tension failure through the minimum section of the stringer blade (Figure 26). Analytical predictions of the failure mode and location correlated precisely with the test results. This test was very successful in that the merits of both the design concept and fabrication methods were demonstrated, and the accuracy of the analysis methodology was verified. Detailed discussions of the analysis methods and analysis/test correlation are presented in Sections 6 and 7.

DEMONSTRATION SUBCOMPONENT TESTS

In addition to the stringer transition specimen, selected portions of the corner joint were tested individually as "subcomponents" of the larger structure. The primary purpose of these tests was to provide additional confidence in the recently developed analytical methods. The subcomponent specimen shown in Figure 27, one of two to be tested, represents the portion of the wing skin and spar cap splice below the aluminum corner fitting. An additional subcomponent specimen (not shown) was tested as a representative portion of the spar and stiffener web sections which were spliced externally by a titanium splice and internally by the aluminum corner fitting. The member thicknesses, fastener sizes, and overall joint geometry of the subcomponent specimens were identical to the corresponding portions of the technology demonstration joint (see the following section, Technology Demonstration Test).

The two demonstration subcomponent specimens were tested in static tension to failure, resulting in net-section tension failures through the first row of fasteners as shown in Figures 28 and 29. The failure modes and locations were correctly predicted analytically. The specimen shown in Figure 28 consisted of two composite plates, each 1/2-inch thick, representing the wing skin and spar cap members. Tapered titanium splice plates were attached on either side of the laminates, and an aluminum tension fitting representative of the demonstration joint corner fitting was mounted above one splice and attached at the specimen centerline with two load-indicating tension bolts. The failure occurred at an applied load of 270,000 pounds. This corresponds to a gross-section stress and strain level of about 47,500 psi and 5,100 microstrain for the composite members.

The smaller subcomponent specimen shown in Figure 29 consisted of a 1/2-inch thick laminate representing the vertical leg of the spar cap, while a thinner laminate roughly 1/3 inch thick represented the stiffener web. In this case, the aluminum fitting is the only means of load transfer on one side of the joint through the tension fastener between fittings. A tapered titanium splice was used on the opposite side.

Failure occurred at an applied load of 115,400 pounds, corresponding to a gross-section stress of 46,200 psi and a strain level of 4,970 microstrain The failure mode was again a net-section failure in the two composite members through the first row of bolts, as shown in Figure 29.

The successful testing of the two subcomponent specimens provided a sufficient level of confidence in both the design approach and analysis methodology to proceed with the design and fabrication of the technology demonstration joint. The analysis of these two specimens included the first attempts at predicting load-sharing through several layers of material in a multirow joint using a semiempirical, finite-element approach. Fastener modeling techniques were modified in order to properly represent the joint load-deflection characteristics at each fastener location (see Section 6) without inducing any additional loads due to secondary effects.

The correlation between strength predictions and test results for the two subcomponent specimens verified the effectiveness of these analytical modeling techniques, and the performance of the two specimens demonstrated the overall design approach. These results provided a sufficient level of confidence in the recently developed methodology to confidently perform the load-sharing analysis and subsequent strength predictions for the larger and more complex technology demonstration specimen.

TECHNOLOGY DEMONSTRATION TEST

The Phase II test program culminated in a static tension test of a large bolted joint representing the lower rear spar and wing skin splice at the side of the fuselage attachment. The original design concept for the test specimen in shown in Figure 30. The composite joint structure consisted of the wing skin, spar cap, and spar web members. All of the splice plates and fittings were made of aluminum and titanium, for the reason discussed in Section 3. The splice members were tapered and fastener sizes were selected in an attempt to optimize the bolt load distributions and maximize the joint strength. The standing leg of the titanium "tee" splice at the specimen centerline represents the attachment to the side of the fuselage bulkhead where the outboard wing structure is spliced to a center wing box.

The specimen presented a challenging task from both an engineering and manufacturing standpoint. In an effort to reduce the complexity and cost of the structural test, the dihedral and sweep break of the actual baseline wing design were not included in the specimen. Nevertheless, the asymmetric nature of the specimen warranted the use of side restraints at the specimen centerline to restrict out-of-plane deflections which would not be present in an actual wing box structure. The specimen end fittings were designed to minimize these effects by adjusting the center' e of applied load toward the test section center of mass. All of the composite joint members were fabricated with the same 10-mil tape material as previous specimens, using the 37.5 percent 0-degree fiber pattern.

The technology demonstration test article is shown in Figure 31 in the process of being assembled. All of the composite joint members were flat plates except for the spar cap members which were angle sections. The spar cap sections were fabricated on an aluminum male tool which had the required thickness transitions machined into the tool surface. Figure 32 shows a closeup view of the joint test section with one side fully assembled. Titanium fasteners were used in all cases and the tapered metallic surfaces were spotfaced to accommodate fastener seating.

The specimen was equipped with 25 axial strain gages to monitor the joint performance throughout the test. The gages were used primarily to measure the load distribution between joint members, although several gages were located along the edges of the members between fastener rows to evaluate the load-sharing between layers. The specimen is shown in Figure 33 with the strain gages attached, ready for installation in the test machine.

The overall test setup is shown in Figure 34. The specimen is attached to the test machine through a standard pin loading arrangement. A dual actuator system with two 500,000-pound-capacity load cells was used to apply the test loads.

The static test began with a limit-load test, during which the specimen was loaded to 300,000 pounds in axial tension followed by a return to zero load. The specimen was then inspected visually and no flaws or damage were found. The test article was then loaded continuously to failure, which occurred at a load of 488,000 pounds. Although this failure load was roughly 92 percent of the predicted strength, the failure was located in the end fitting area away from the joint test section. A closeup view of the failure is shown in Figure 35. This view shows that the spar cap member was actually delaminated from the thickness buildup on the inner surface of the cap to the first row of fasteners in the end fitting, where a net-section failure occurred in the reduced thickness of the spar cap member. The skin and spar web members failed through the first row of field fasteners toward the joint test section.

It is not possible to verify the exact cause of failure. However, it does appear that the failure was, in fact, initiated by the delamination of the spar cap member. Once this delamination extended to the first row of fasteners in the end fitting, the effective thickness at the net-section was reduced by approximately one-third to a level which was insufficient to carry the test loads. Once the initial failure of the spar cap occurred, the first row of field fasteners became a point of high load transfer and the final failure of the skin and spar web members took place. The end fitting failure is graphically represented in Figure 36.

A close inspection of the failed members after the test substantiated the initial observations and conclusions regarding the cause and mode of failure. (It should be noted that c-scan results for the failed spar cap member prior to the test did produce some questionable results in the region of the delamination.) A typical c-scan of the joint test section taken after the test is shown in Figure 37. Scan results indicate that irreversible damage in the opposite-side spar cap members had taken place, and that the joint test section was close to failing when the premature end fitting failure took place. After reviewing the possible program options, it was decided to refurbish the failed specimen and conduct another static test. This effort was conducted using Douglas development funds.

After complete visual and nondestructive inspections of the unfailed composite members were completed, the specimen was reassembled using two 7075-T6 aluminum plates to replace the failed composite members. The aluminum parts were machined to the exact thicknesses of the original composite parts, both in the joint test section and the end fitting areas. The refurbished test article, with a view of the aluminum replacement parts, is shown in Figure 38.

Another static test was then conducted, this time with excellent results. The specimen failed at an applied load of 484,420 pounds with both the failure load and location showing good correlation with analytical predictions. The maximum strain in the composite members, occurring in the spar cap section, was roughly 5,000 microstrain. This corresponds to a far-field stress level of about 46,500 psi. The failure

was a net-section tension failure through the first (outermost) row of fasteners in the joint test section, as shown in Figures 39 and 40. The skin, spar cap, and spar web members all failed through this location.

A comparison of the results for the two static tests of the demonstration component may, at first, seem somewhat surprising. The failure load of the second test was nearly equal to (in fact, slightly less than) that of the initial test, which resulted in the premature end fitting failure. However, based on the results of the strain gage measurements, there was a greater difference in strain level between the skin and spar members during the second test than during the first. In each test, the spar cap member was carrying slightly more of the applied load than the skin, but this difference was more pronounced in the second run.

Thus, for the same level of applied load, the spar cap member was working to roughly a 10-percent higher stress level than the skin in the second test, leading to the slightly lower failure load. This phenomenon is a likely cause for the failure having occurred at a slightly lower load level than had been analytically predicted, as will be discussed further in Section 7.

The entire technology demonstration test program is fully reported in Reference 10, including load-strain plots for all strain gage measurements taken throughout each test. The test program results are summarized in Table 1.

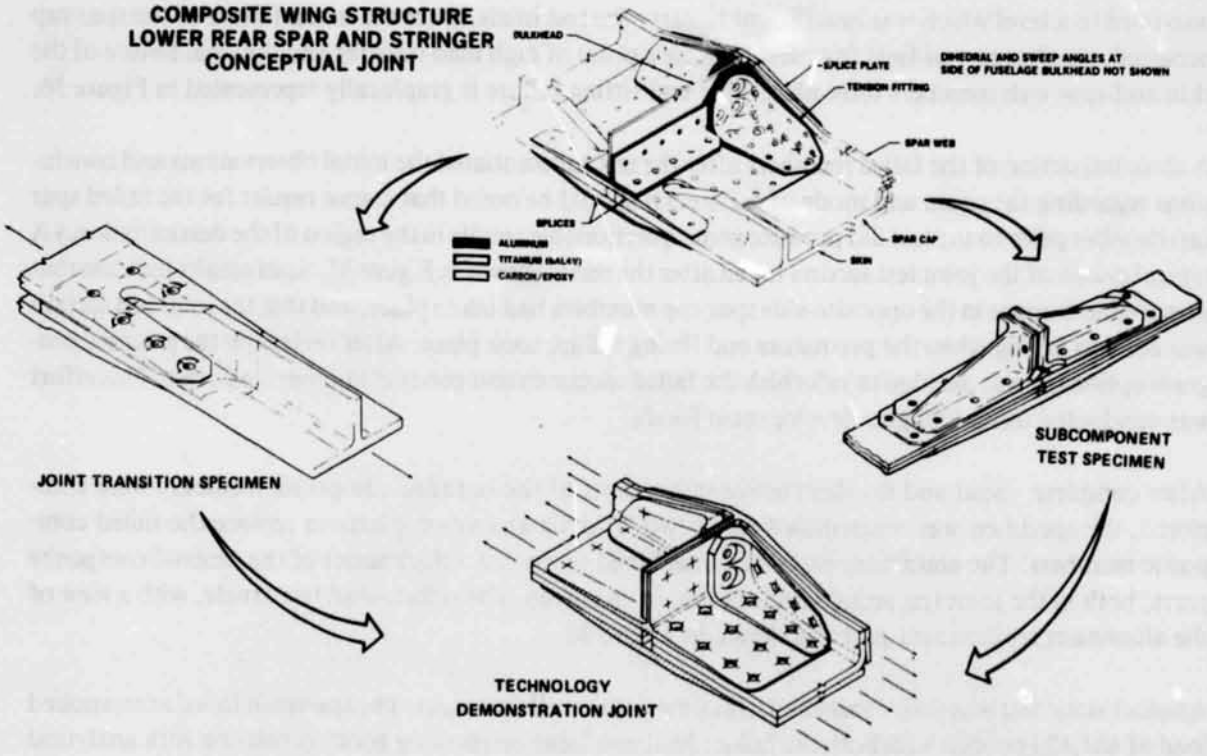

FIGURE 22. PHASE II TEST PROGRAM

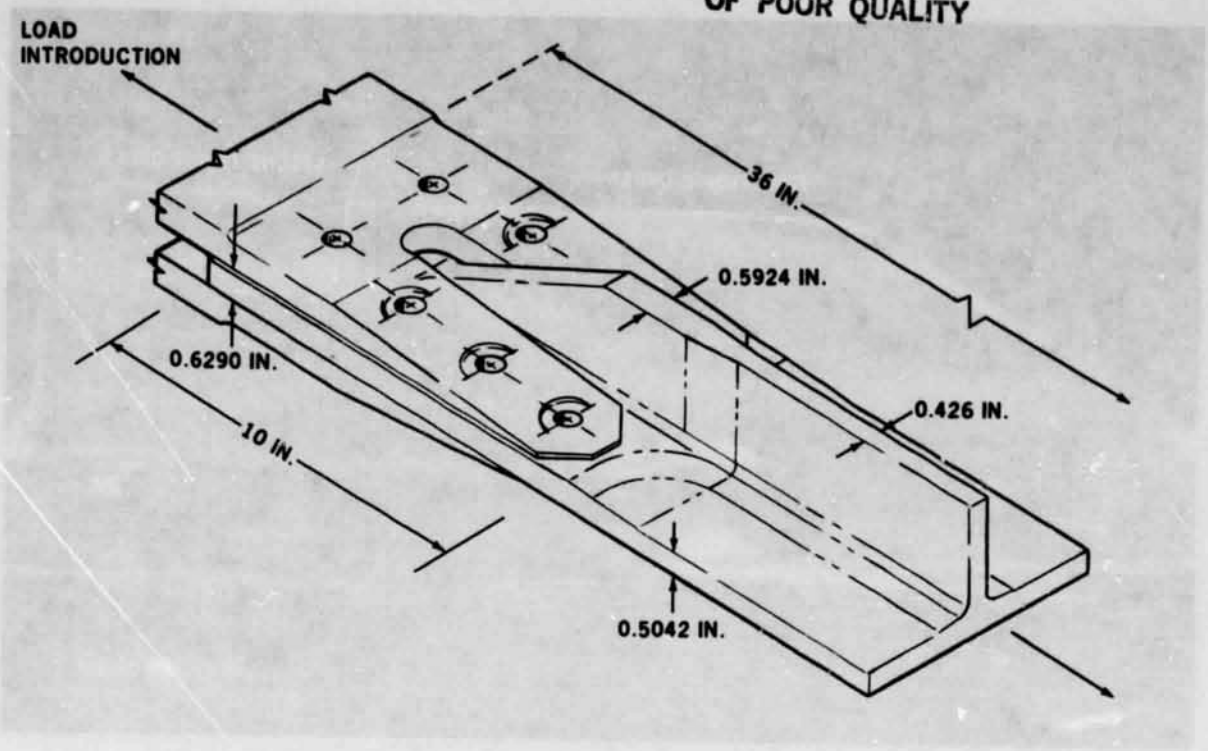

FIGURE 23. STRINGER TRANSITION JOINT DESIGN CONCEPT

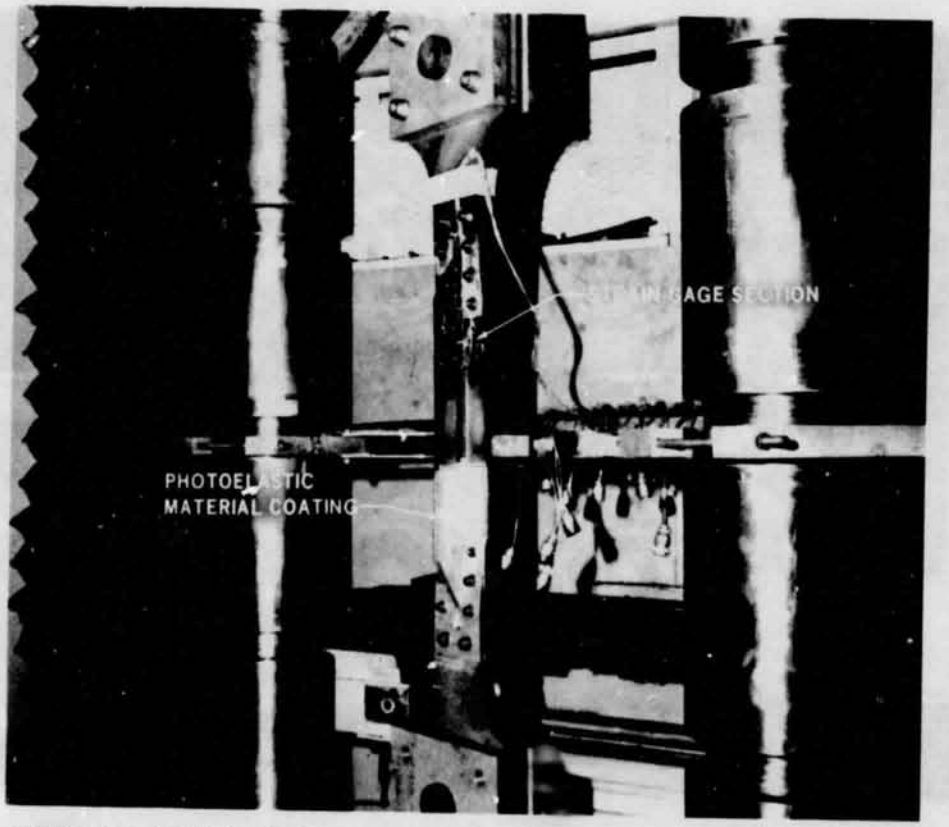

FIGURE 24. STRINGER TRANSITION SPECIMEN INSTALLED IN TEST MACHINE

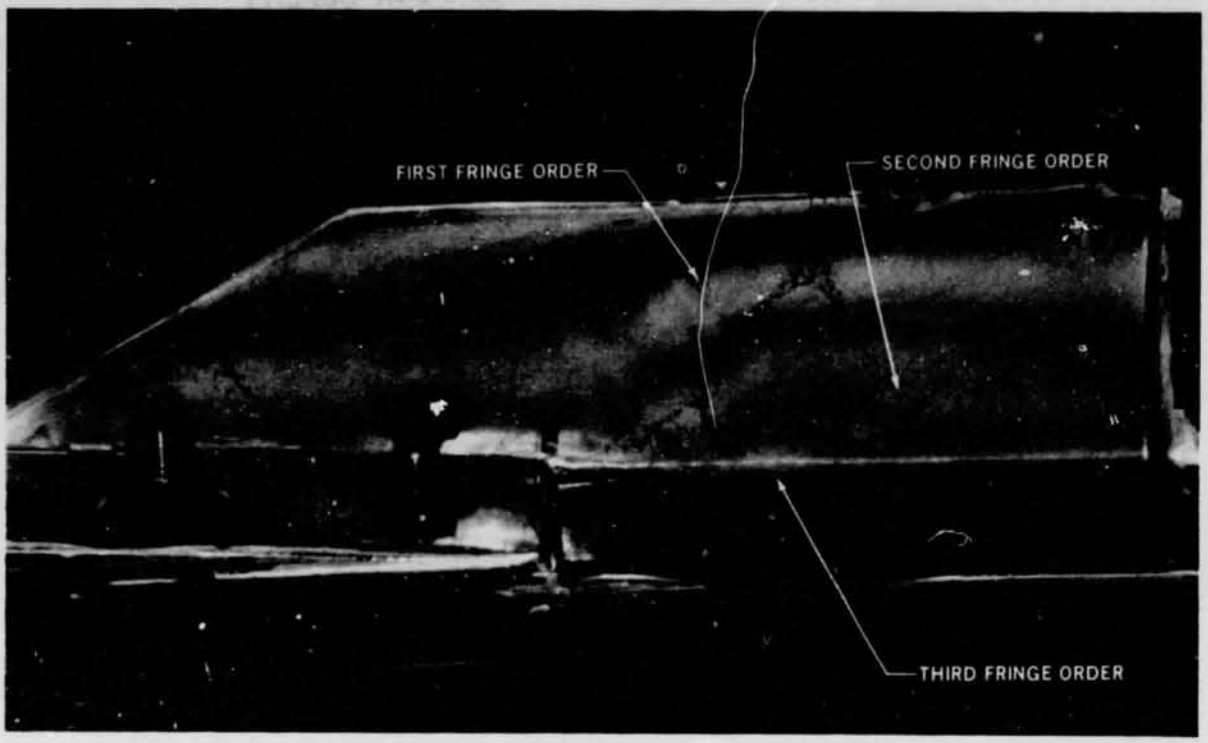

FIGURE 25(a). PHOTO-ELASTIC SURVEY – STRINGER BLADE, APPLIED LOAD = 80,000 POUNDS

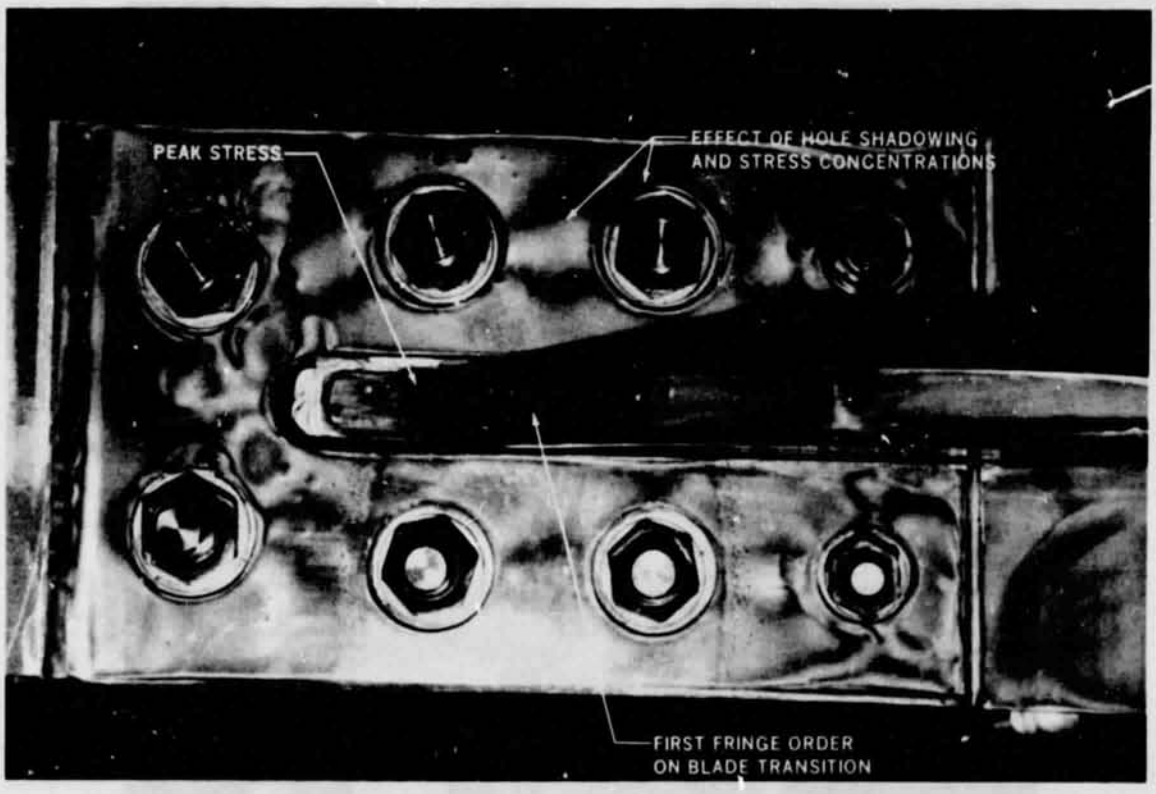

FIGURE 25(b). PHOTO-ELASTIC SURVEY – UPPER SPLICE, APPLIED LOAD = 80,000 POUNDS

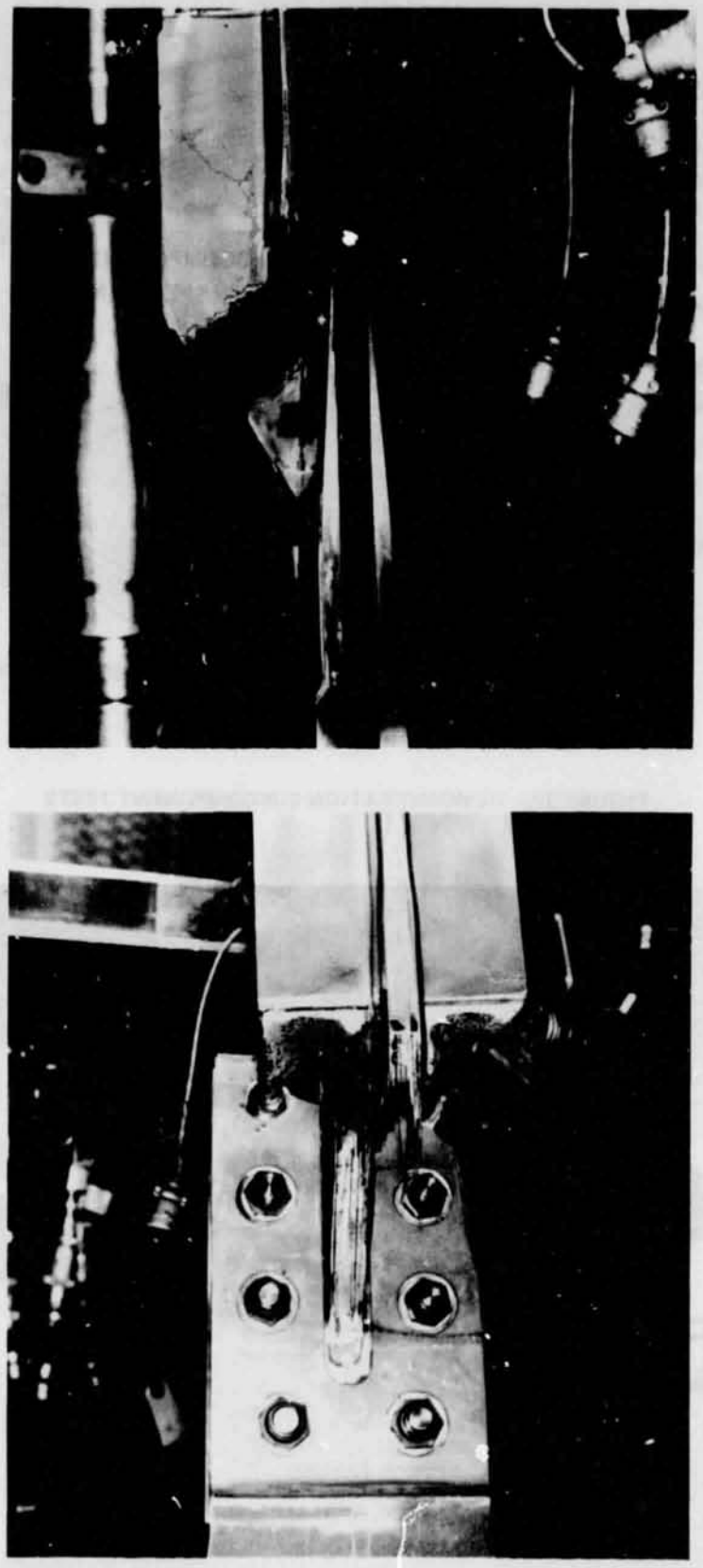

FIGURE 26. STRINGER TRANSITION TEST – FAILED SPECIMEN

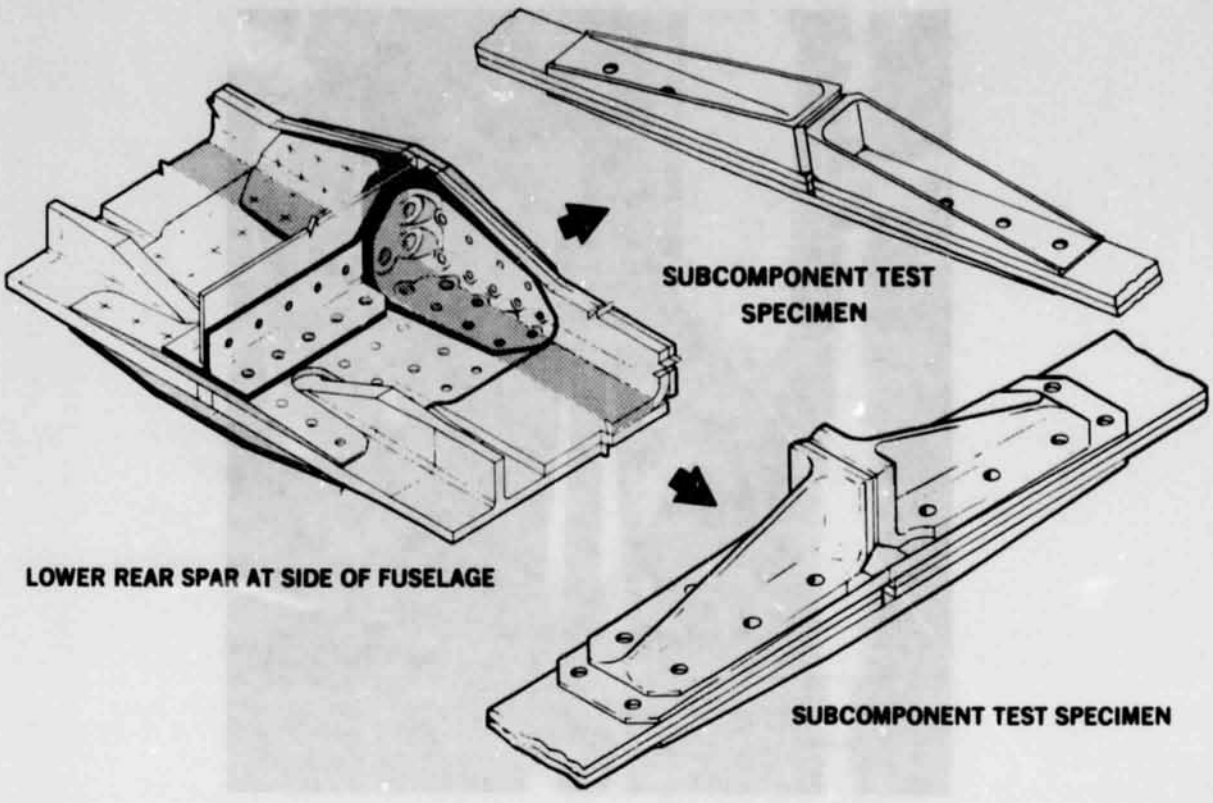

FIGURE 27. DEMONSTRATION SUBCOMPONENT TESTS

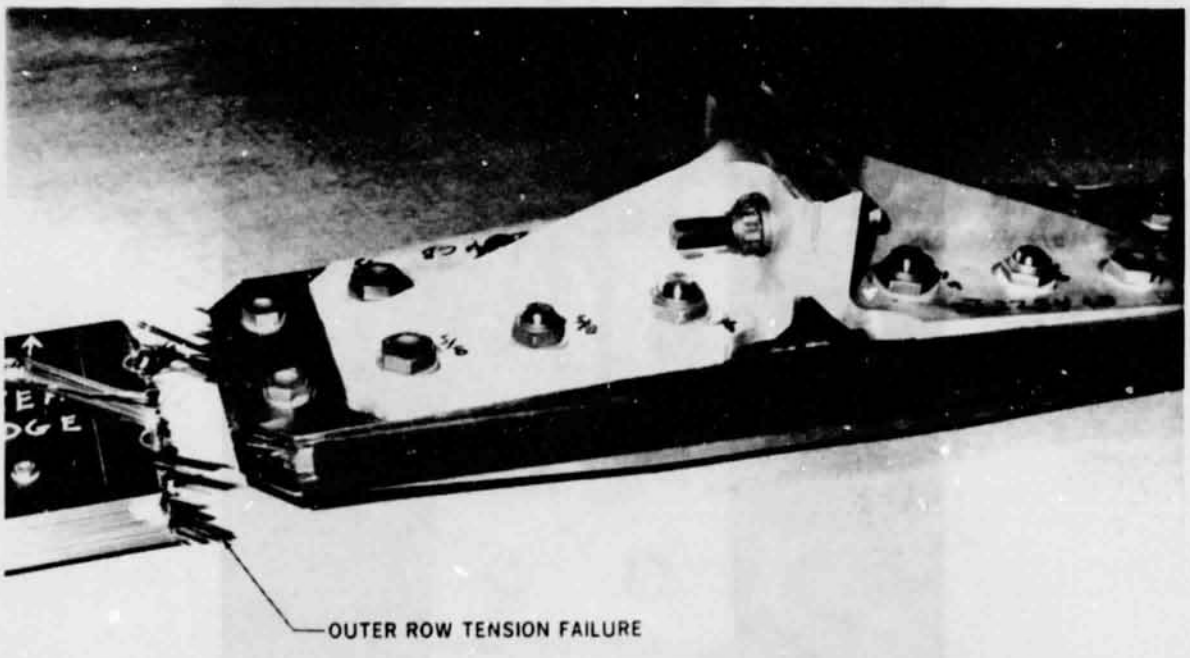

FIGURE 28. SUBCOMPONENT NO. 1 – FAILED SPECIMEN

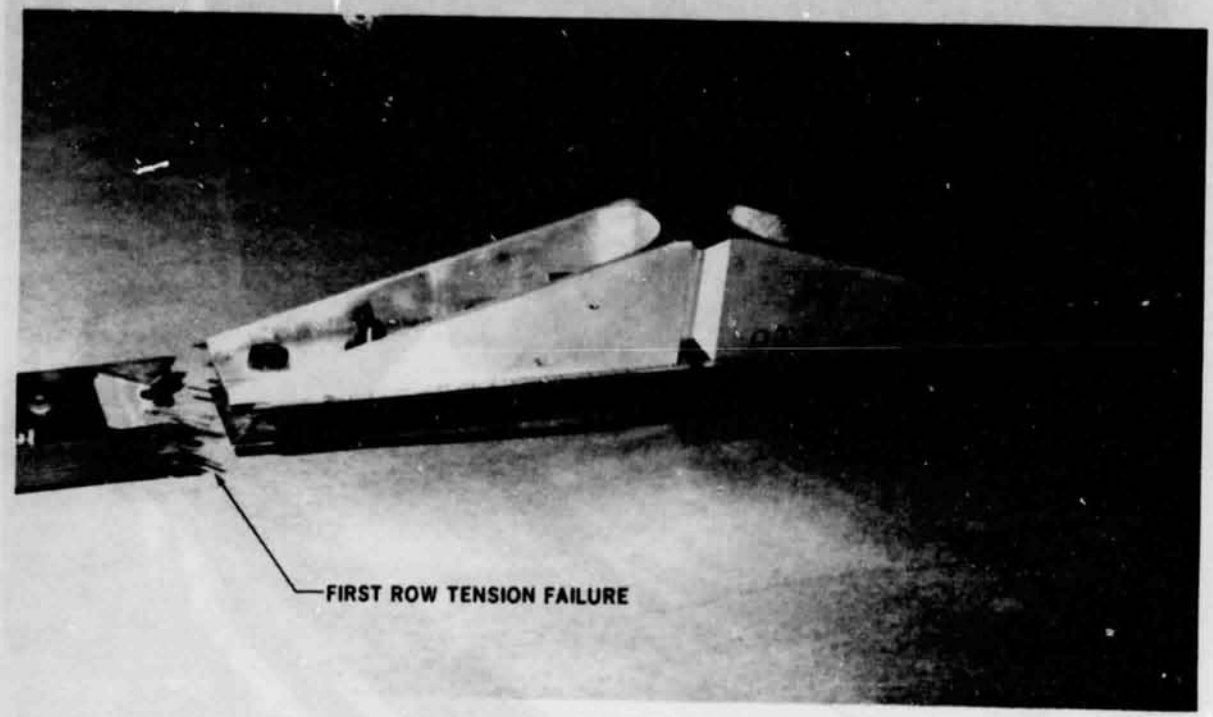

FIGURE 29. SUBCOMPONENT NO. 2 – FAILED SPECIMEN

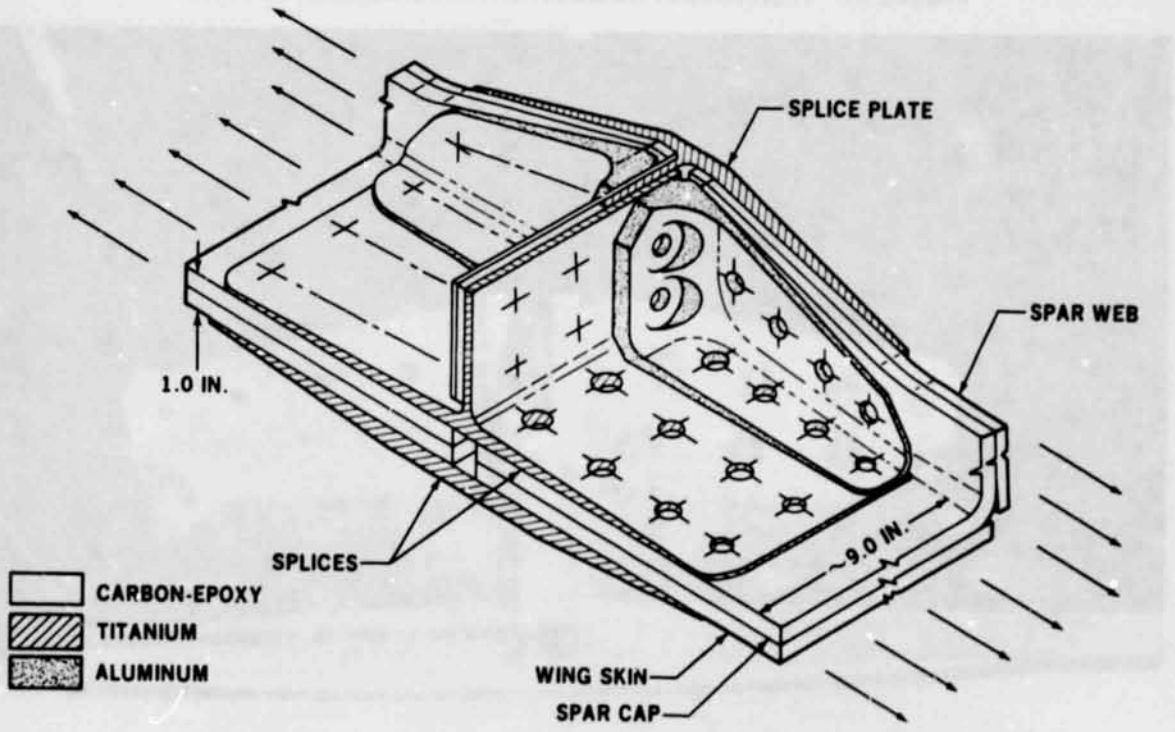

FIGURE 30. TECHNOLOGY DEMONSTRATION JOINT DESIGN CONCEPT

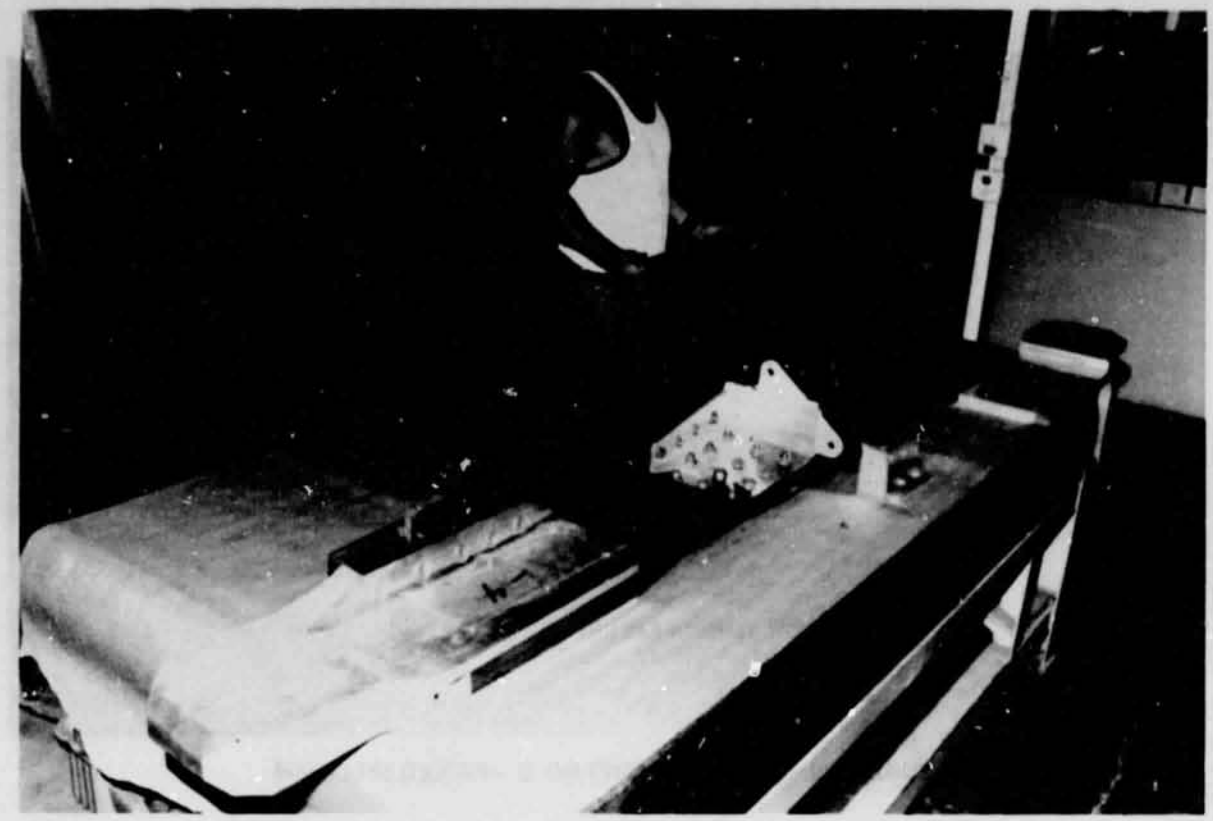

FIGURE 31. TECHNOLOGY DEMONSTRATION SPECIMEN ASSEMBLY

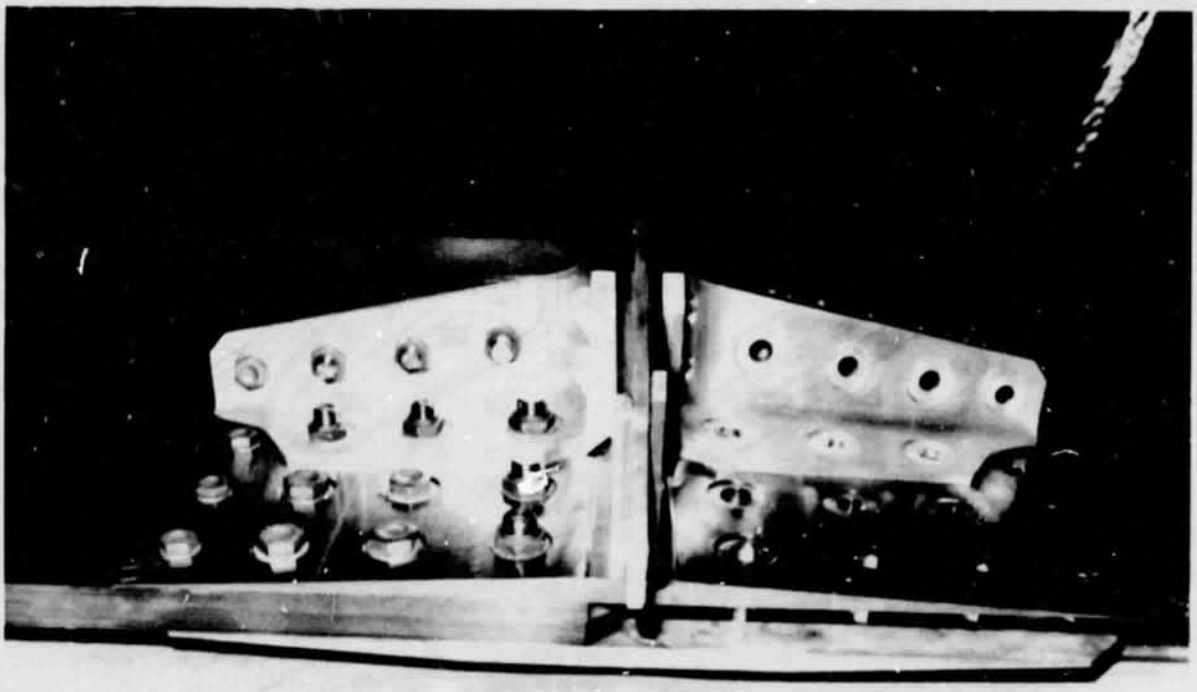

FIGURE 32. TECHNOLOGY DEMONSTRATION SPECIMEN – TEST SECTION

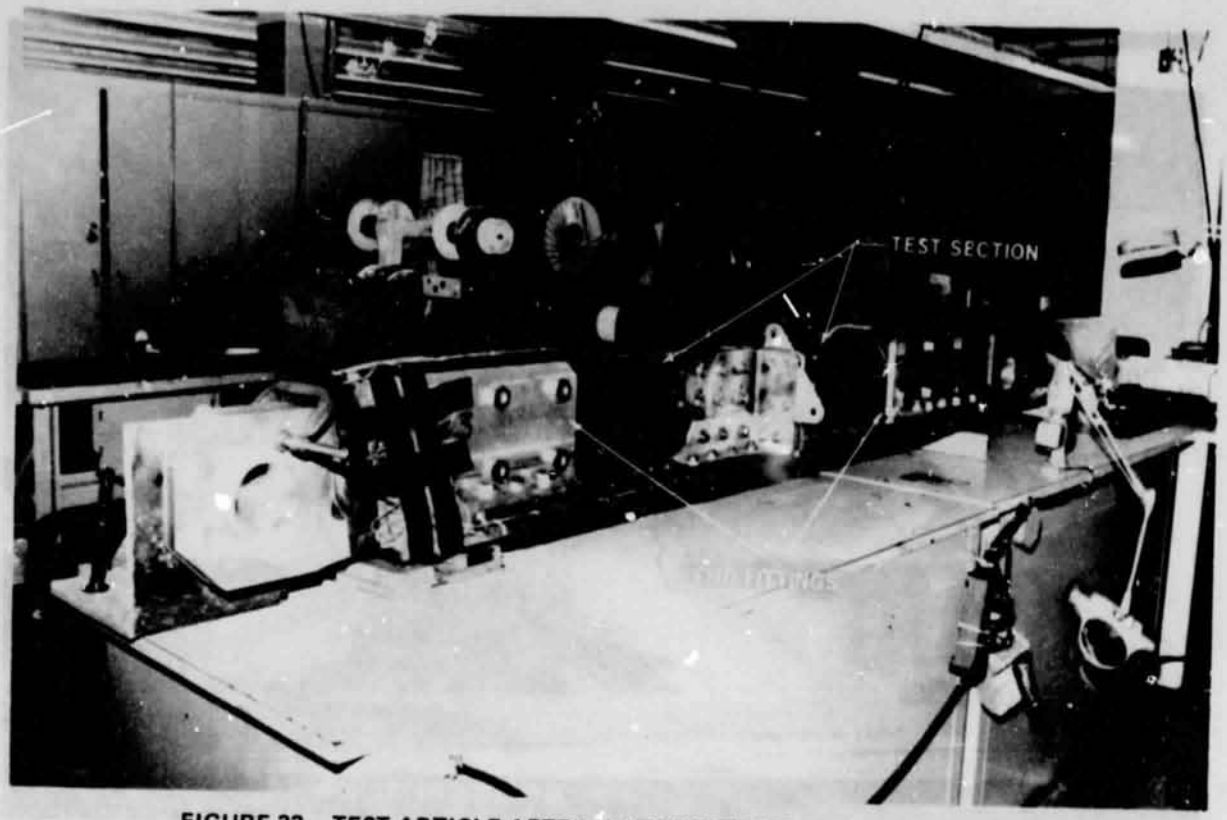

FIGURE 33. TEST ARTICLE AFTER INSTRUMENTATION – SPAR CAP SIDE

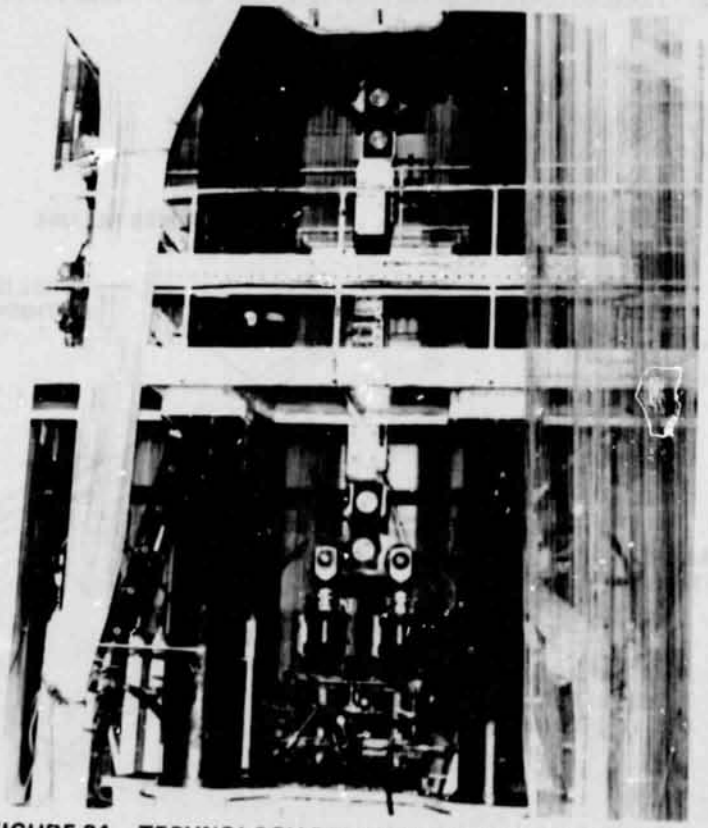

FIGURE 34. TECHNOLOGY DEMONSTRATION TEST SETUP

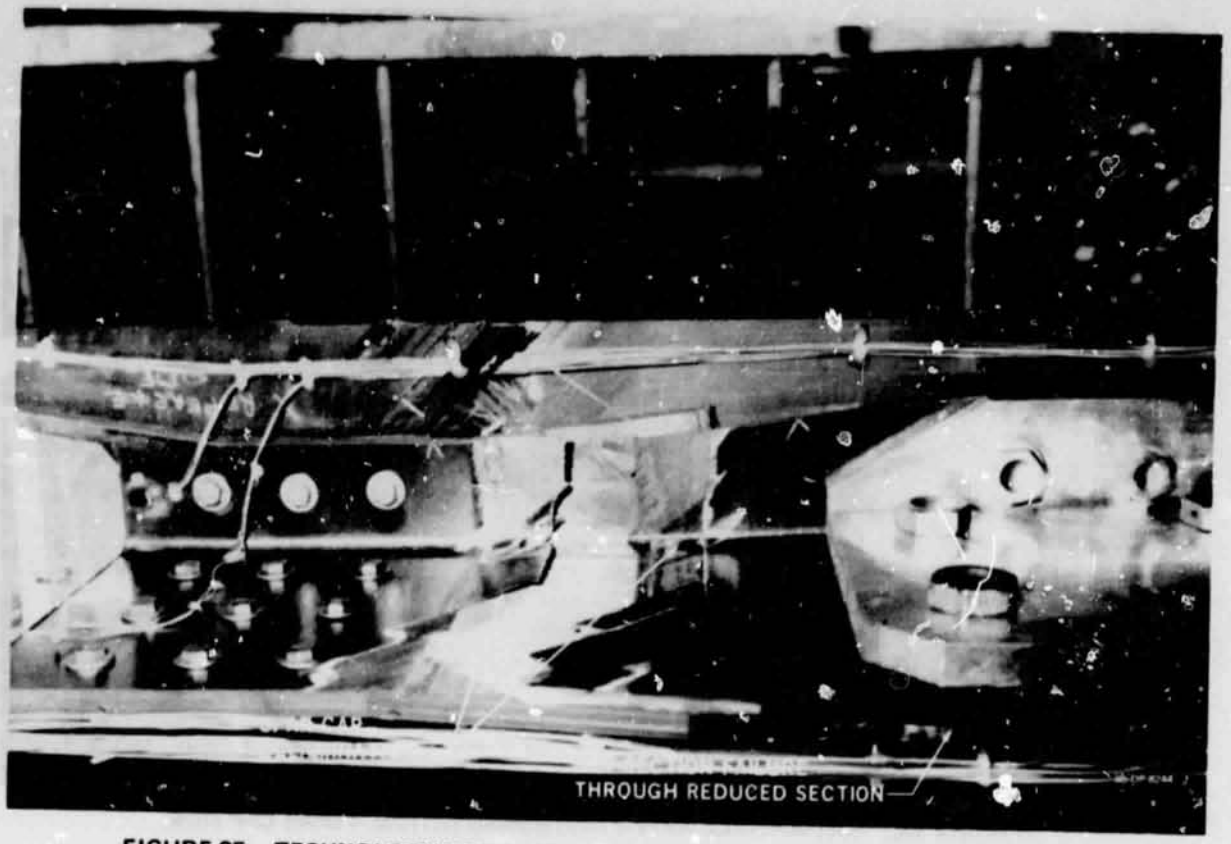

FIGURE 35. TECHNOLOGY DEMONSTRATION TEST NO. 1 – END FITTING FAILURE

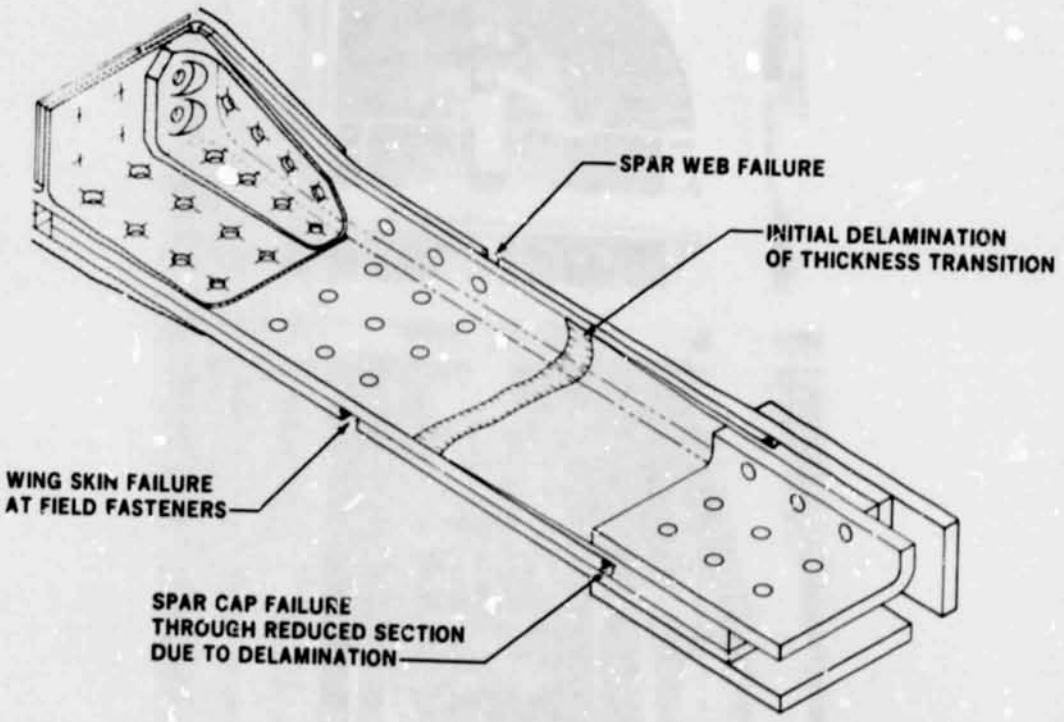

FIGURE 36. TECHNOLOGY DEMONSTRATION TEST – END FITTING FAILURE

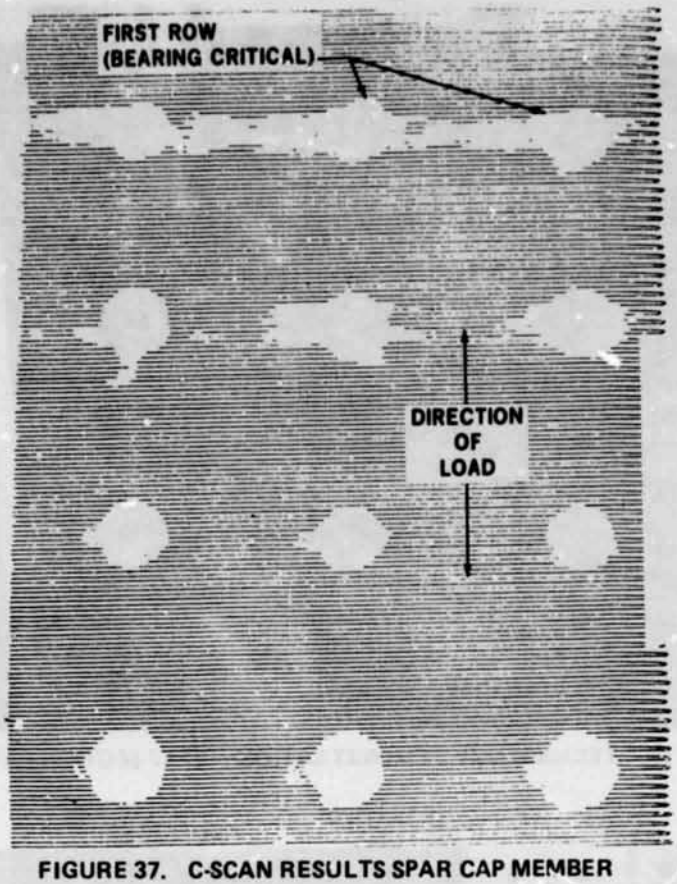

FIGURE 37. C-SCAN RESULTS SPAR CAP MEMBER

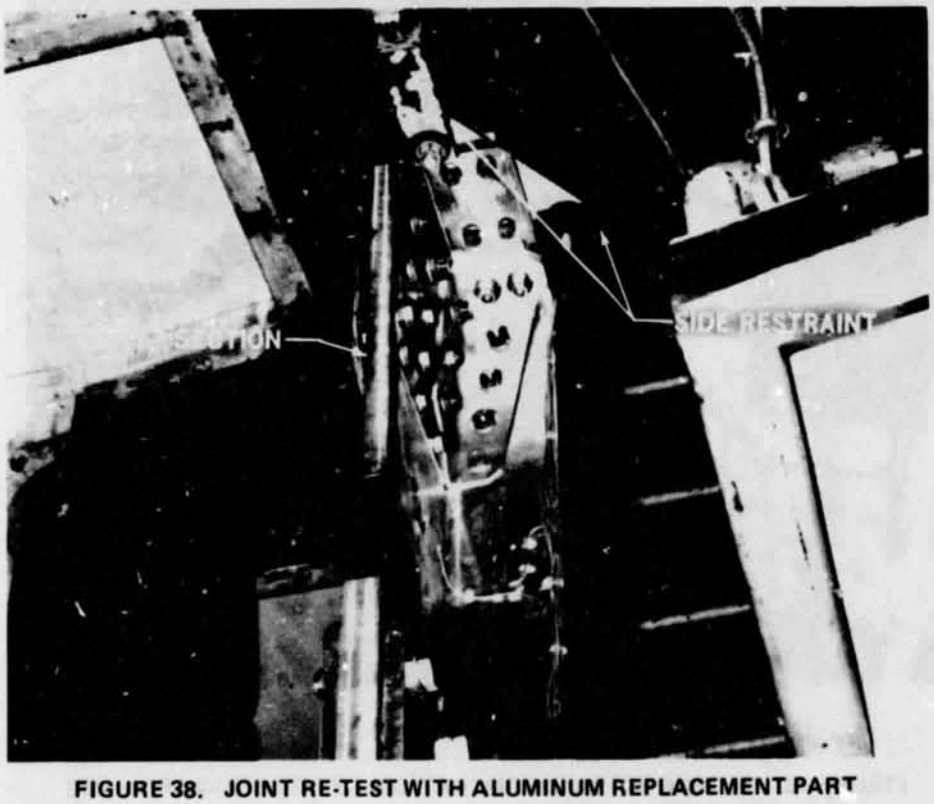

FIGURE 38. JOINT RE-TEST WITH ALUMINUM REPLACEMENT PART

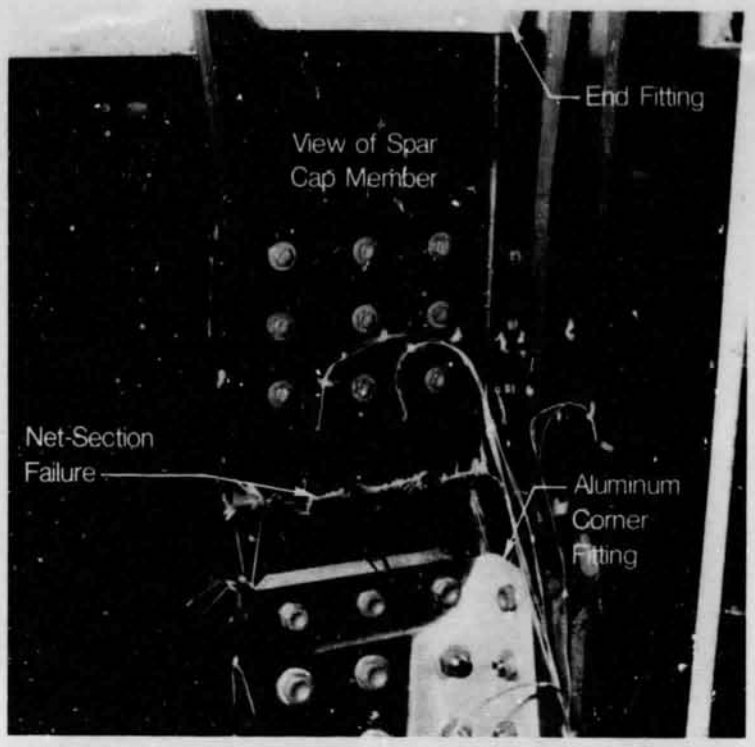

FIGURE 39. TECHNOLOGY DEMONSTRATION – TEST SECTION FAILURE

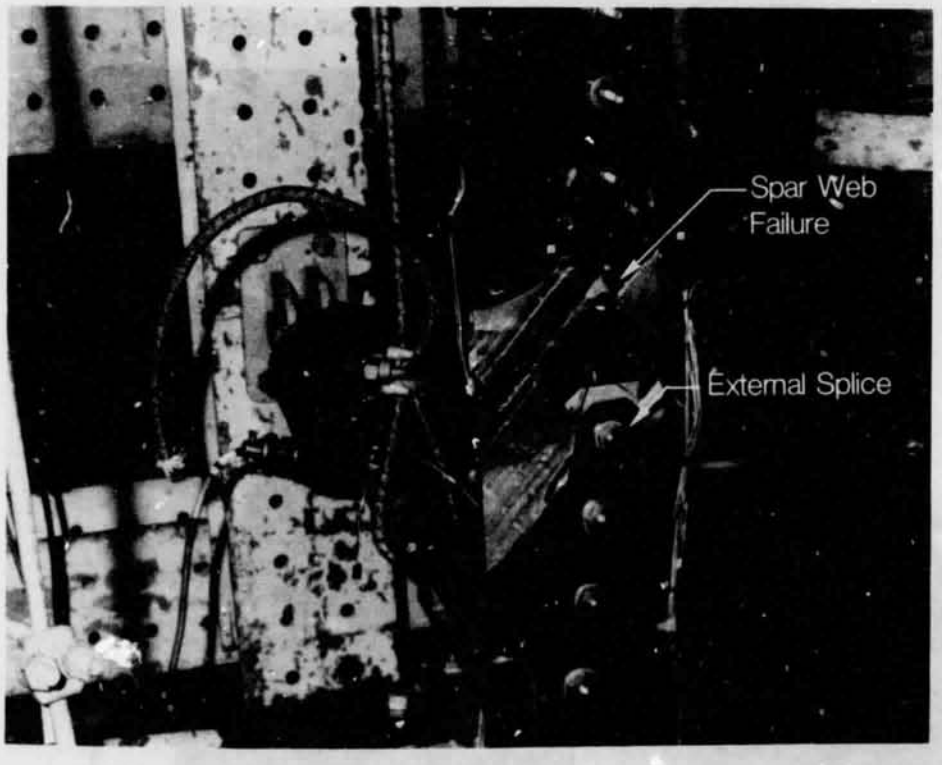

FIGURE 40. TECHNOLOGY DEMONSTRATION – TEST SECTION FAILURE

TABLE 1
PHASE II TEST PROGRAM
TECHNOLOGY DEMONSTRATION TEST RESULTS

TEST SPECIMEN	FAILURE LOAD (LB)	PREDICTED STRENGTH (LB)	GROSS-SECTION STRESS AT FAILURE (PSI)	GROSS-SECTION STRAIN AT FAILURE (MICROSTRAIN)	PREDICTED STRAIN LEVEL AT FAILURE (MICROSTRAIN)	FAILURE MODE
STRINGER TRANSITION	197,200	183,700	50,000*	5,891 4,700**	5,945 4,800	NET-SECTION TENSION
SUBCOMPONENT NO. 1	270,000	260,000	47,500	5,100	4,920	NET-SECTION TENSION
SUBCOMPONENT NO. 2	114,400	90,000***	46,200	4,970	3,900***	NET-SECTION TENSION
TECHNOLOGY DEMONSTRATION ARTICLE TEST NO. 1	488,000	531,000	43,700 (SKIN) 45,600 (SPAR)	4,700 (SKIN) 4,900 (SPAR)	5,110 (SKIN) 5,330 (SPAR)	END FITTING
TECHNOLOGY DEMONSTRATION ARTICLE TEST NO. 2	484,400	531,000****	42,800 (SKIN) 46,500 (SPAR)	4,600 (SKIN) 5,000 (SPAR)	5,110 (SKIN) 5,330 (SPAR)	NET-SECTION TENSION

*AVERAGE STRESS IN BASIC SECTION PRIOR TO THICKNESS BUILDUP
**CALCULATED STRAIN LEVEL AT BOLTED JOINT AFTER THICKNESS BUILDUP
***REFER TO DISCUSSION — PAGE 54
****REFER TO DISCUSSION — PAGES 54 AND 55

85 DP 8254

SECTION 6
ANALYSIS METHODOLOGY DEVELOPMENT

The analytical methods developed during Phase I were sufficient for the analysis of multirow joints of uniform cross-section, or for structures where geometric variations have a minimum influence on the bolt load distributions. Load-sharing analyses using the A4EJ computer program were proven to give accurate results for the prediction of the bolt load distributions and failure loads for the two-row and four-row joints tested in Phase I. The program can predict the load-sharing between fasteners both at the limit of elastic (linear) behavior and after the load redistribution associated with any noncatastrophic initial damage. An iterative solution is performed for the load-sharing between multiple parallel springs (fasteners) and also accounts for the linear or nonlinear deformations of the joint members between fasteners as sets of springs in series. The details of the mathematical model on which the A4EJ solution is based are described in Figure 41.

Strength cutoffs are input to the program for the fasteners in shear or bending, and for the joint members under combined bearing and bypass loads at each fastener location. The bearing-bypass interaction curves are developed empirically, as discussed in Section 4. Much of the methodology development effort during Phase II focused on refining the methods for establishing these strength cutoffs, such as the chart presented earlier in Figure 21 which defines bolt bending allowables as a function of joint geometry.

Although solutions using the A4EJ program were accurate for the analysis of Phase I subcomponent joints, the more complex joints of Phase II required a more versatile analysis approach. Accurate load-sharing analyses of structures which have substantial geometric variations in the joint region cannot be performed with simple strip solutions. The A4EJ program is also limited to single-shear or double-shear joints with uniaxial loading. Actual structure is often more complex, with biaxial or triaxial stress states and multiple layers of material. The need for a more comprehensive analysis method became evident when considering the analysis approach to be used for the stringer transition specimen. The concept (Figure 23) carries the stringer blade well beyond the first row of fasteners in the bolted joint before transitioning into the skin. While simple analyses using the A4EJ program can provide an estimate of the joint performance, an accurate load-sharing analysis must account for the amount of "bypass" load in the stringer blade versus the bypass load at each fastener hole.

The selected approach was to combine a finite element analysis model with the semiempirical methods developed throughout the program. The concept, illustrated in Figure 42, was to use a finite element model to perform the load-sharing analysis, while the strength cutoffs would still be determined semi-empirically. Figure 42 shows a representation of the finite element model used in the analysis of the stringer transition specimen. The model was constructed using the NASTRAN finite element code, with isotropic and anisotropic elements used to model the metallic and composite members, respectively.

Laminate stiffness and unnotched strength properties were calculated on a ply-by-ply basis. The fasteners were represented by bending bars with properties which would provide the correct load-deflection properties (elastic spring rates) based on calculations using the existing semiempirical methods. Bearing-bypass load combinations determined by the model at each fastener location are then compared to empirically derived interaction curves for failure prediction. Nonlinear effects are accounted for through successive iterations with altered stiffness properties, based on the same bilinear

representation of the load-deflection properties at each fastener. Customary failure criteria are used for the unnotched portions of the structure.

There is often a tendency to use finite element analysis methods at excessive levels of detail, resulting in unnecessarily high costs. It was therefore an objective of the analysis development effort to perform accurate strength predictions while minimizing the complexity of the approach. Since the stringer transition joint was the first to be tested, a relatively coarse grid model was constructed to model its behavior. It should be noted that the finite element model was not used to examine the stress concentration effects at the fastener holes. The bearing-bypass curves determined by semiempirical methods fully account for these effects, so the finite element model need only perform the load-sharing analysis to determine bolt load distributions.

The initial modeling approach shown in Figure 42 had the fastener elements attaching directly to the plate elements which represented each joint member. At first, no material was removed where the fastener holes were located. This approach was eventually shown to be somewhat oversimplified for several reasons. In the case of the stringer transition analysis, the amount of bypass load on either side of the fastener hole was critical to performing an accurate strength prediction. (See discussion of analysis/test correlation for stringer joint in Section 7.) In addition, the stiffness of the joint members are more correctly represented by removing material for the fastener holes.

This approach also facilitated the modeling of fasteners for the analysis of the demonstration subcomponent specimens and the technology demonstration article. By removing the material at the fastener holes, the bolts are more readily represented through multiple layers of material and can easily be modeled to account for biaxial or off-axis loading. The individual fasteners are represented by simple bending bars which are given bending stiffness properties derived from load-deflection calculations or from single-row test results.

Following the analysis of the stringer transition joint, all subsequent analysis models reflected the refinements discussed above. An exploded view of the finite element model used for the analysis of the technology demonstration specimen is shown in Figure 43. This model is somewhat more detailed than the stringer joint model, particularly in the region of fastener holes where a reasonable representation of the true net-section area (stiffness) was desired. The analytical model was reacted at the test specimen centerline and uniform displacements were enforced on the skin, spar cap, and spar web members to generate the applied tension loads.

The key to this analysis approach is the use of finite element analysis in combination with semiempirical methods. By using the finite element model to perform only the load-sharing analysis, the model complexity and cost can be kept to a minimum. More detail can be used where correlation with strain gage data is required, or for structural details or areas of potentially high stress intensity other than the bolted joint which require a detailed stress analysis. The orthotropic elements of a NASTRAN can properly account for any biaxial effects, which may otherwise be difficult to predict with simpler methods when highly orthotropic fiber patterns are used. Although methods for determining bearing-bypass interaction curves under biaxial loads have not been presented here, any method such as the BJSFM program (discussed earlier) can be used, in conjunction with the load-sharing analysis model, to calculate the strength envelopes at each fastener location.

The following section will present the correlation between the analysis and test results for the multirow joints tested in Phase II. While good correlation is shown in each case, the intent here is not to replace the simpler analytical methods with the more complex approach using finite elements. The most simple and cost effective analysis method that will result in accurate strength predictions should always be selected, depending of course on the complexity of the structure to be analyzed.

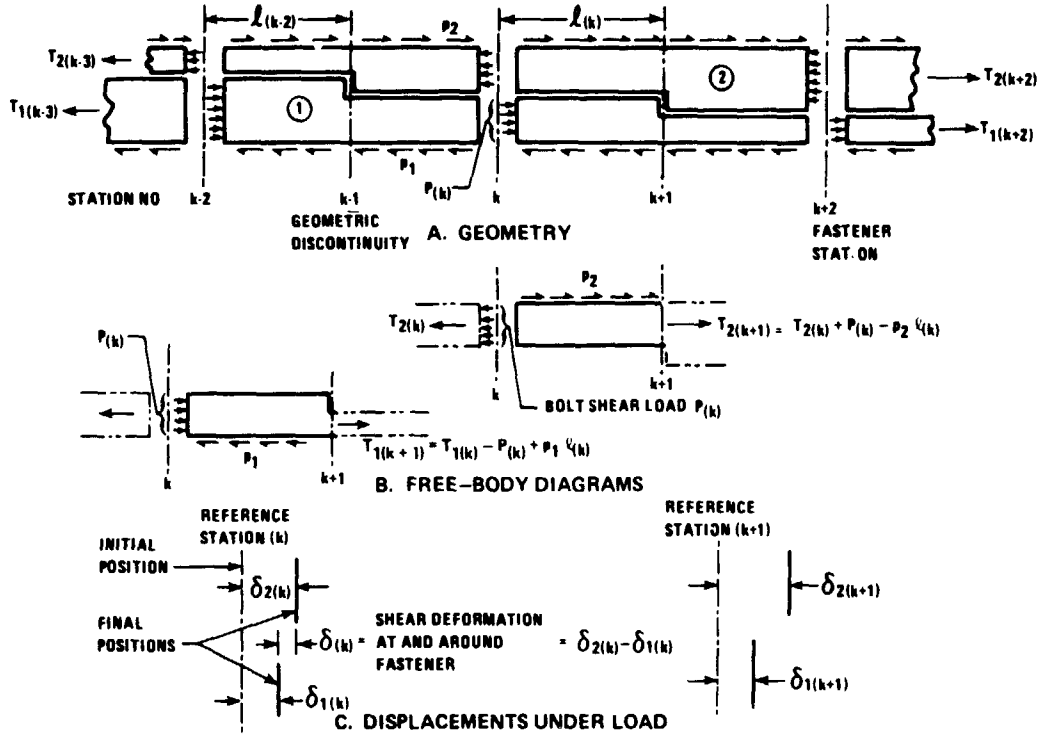

FIGURE 41. LOADS AND DEFORMATIONS ON ELEMENTS OF BOLTED JOINTS

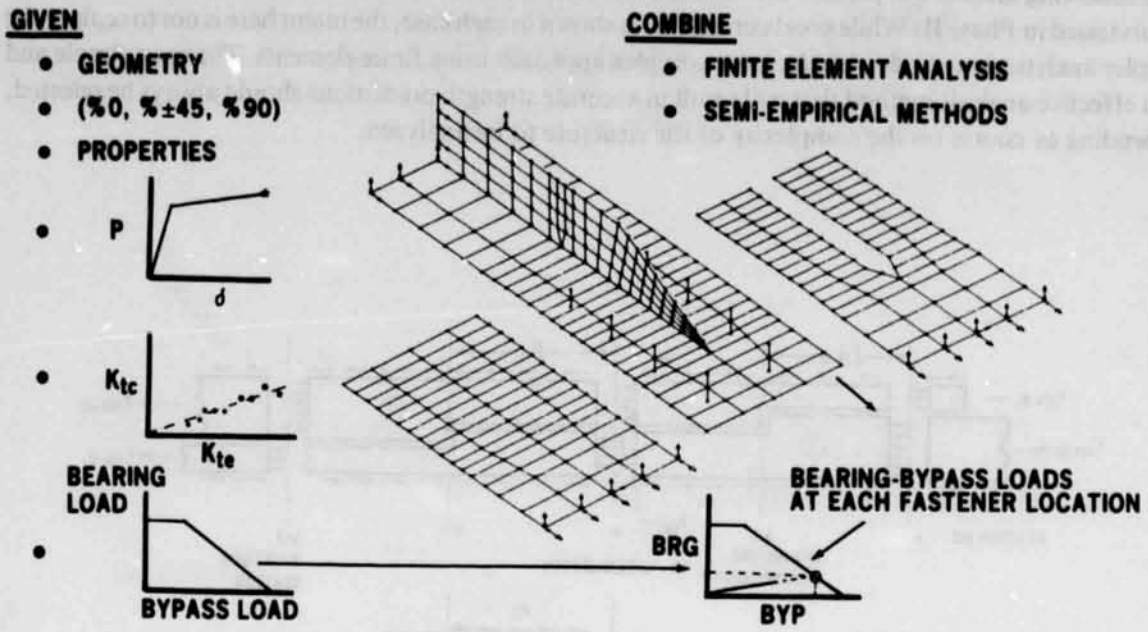

FIGURE 42. STRINGER TRANSITION JOINT ANALYSIS MODEL

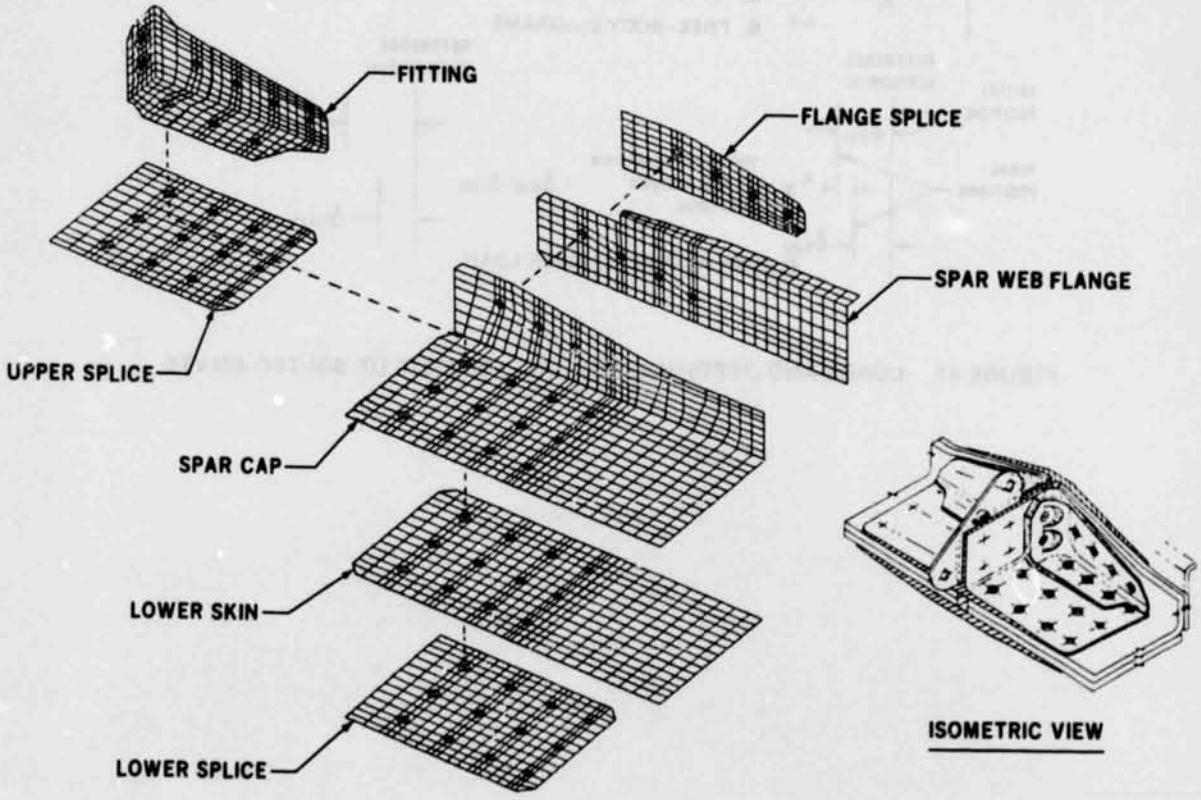

FIGURE 43. EXPLODED VIEW OF ANALYSIS MODEL

SECTION 7
ANALYSIS/TEST CORRELATION

Finite element analyses were combined with semiempirical methods to make strength predictions for each of the four multirow joints tested in Phase II. The finite element models were used to determine the load-sharing between joint members and the bolt load distributions in the joint itself. In some cases, the models were used to predict strain levels for specific portions of each joint member. Bearing-bypass loads from the finite element solutions were compared with semiempirically derived interaction curves to predict the failure load for each specimen. In general, good correlation was demonstrated between analytical predictions and test results. Average data from ancillary tests were used for input to the multirow analyses.

The joint transition specimen analysis was based on the NASTRAN finite element model shown in Figure 42 which was used to determine the stress distribution in the composite skin and stringer blade and to solve for the load-sharing between rows of fasteners. Two iterations were required to account for the change in stiffness (nonlinearily) due to a predicted bearing yield in the titanium splice plates at the first row of fasteners.

As discussed in Section 6, the finite element approach was necessary for this analysis to properly account for the amount of load carried in the stringer blade beyond the first row of fasteners in the bolted joint. This concept is illustrated graphically in Figure 44. The amount of load passing through the stringer blade at point C must be determined by the finite element model in order to predict the loads in the skin at points A and B which bypass the fastener hole. This effect must be accounted for at each fastener location so that strength checks can be made using the proper bearing-bypass load combinations, which are then compared to the associated interaction curves.

The nature of the stringer transition structure is such that there may be a difference in the amount of load transferred around the hole at points A and B. Since there is a substantial difference in the net area and the stress concentration effects between the inner and outer sides of the fastener hole, this difference in load (if any) must also be determined before an accurate strength prediction can be made.

The completed analysis solution predicted a net-section tension failure through the first row of fasteners at an ultimate load of 183,700 pounds (Figure 45). This predicted strength is roughly 5 percent below the tested value of 193,200 pounds. The predicted failure mode correlated precisely with the test results, as described earlier in Section 5. The strain level in the composite skin away from the joint (before the buildup in thickness) was monitored throughout the test. The measured strain at failure of 5,891 microstrain is quite close to the predicted value of 5,945. This corresponds to a difference of roughly 500 psi between the predicted stress level at failure of 55,290 psi and the tested stress level of 54,790 psi.

Analysis models were constructed for each of the two subcomponent specimens, with each joint member represented in its actual geometry. The modeling approach was modified for these two specimens to more properly represent the fastener holes by removing material from each plate element in an amount roughly equal to the area of the bolt hole. This gave a more accurate model of the joint member stiffnesses and allowed the use of a revised approach for modeling the fasteners. The new approach consisted of bending elements representing the bolts with axial bars attached at each end to react the shear load transfer to the joint members. This method allowed the simplest means for modeling the fasteners

through several layers of material. Since the stress concentration effects due to the fastener holes need not be examined by the finite element model, the holes can be represented in a gross sense, with a minimum of detail.

The analysis results for the subcomponent joint representing the wing skin and spar cap members are illustrated in Figure 46. A net-section tension failure through the first row of fasteners was predicted to occur at an ultimate load of 260,000 pounds. This failure mode correlates precisely with the test results (Figure 28), and the strength prediction falls within 4 percent of the tested value of 270,000 pounds. These two values are easily within the range of results that may result from variations in material properties and fastener hole tolerances. Strain readings were taken at selected locations throughout the joint and were compared with predicted strain levels from the analytical model with generally good correlation. (A complete set of load versus strain plots including the predicted values are contained in Reference 10.)

The small subcomponent representing the spar cap and spar web members was analyzed in a similar fashion, with the predicted failure mode again being a net-section failure through the first fastener row. Although this correlated well with the test results (Figure 29), the predicted strength was about 28 percent below the tested failure load. After reviewing the finite element results for this analysis, it was found that the model was predicting a substantial difference in strain level between the two composite members. Intuitively, this was not a logical result, and it was eventually determined that the end conditions of the test specimen had not been properly represented. This allowed unrealistic deformations to take place, resulting in the overly conservative analysis result.

Based on the analysis correlation achieved to this point in the program, the same techniques were used to perform the strength analysis for the technology demonstration article. Although the demonstration article was more complex than previous specimens, the loading was primarily uniaxial and the bearing-bypass curves based on existing ancillary data were again used as the failure criteria for each fastener hole along with the bolt shear and bending allowables. The magnitudes of the bearing and bypass loads at each fastener were extracted from the model and compared to the corresponding interaction curve. The results of this evaluation indicated that the critical location was the first (outermost) row of fasteners in the wing skin member, although the spar cap member was very close to its predicted failure load for the same applied load level. The predicted ultimate load was 531,000 pounds.

The completed analysis indicated that some nonlinear effects were anticipated prior to failure. A slight amount of bearing yield at several locations in the titanium splice plates was predicted at load levels just below ultimate, and far above what could be considered limit load. The failure of the second static test actually occurred at an applied load of 484,420 pounds, roughly 92 percent of the predicted strength. The bearing-bypass curve presented in Figure 47 shows the test results and analytical predictions for the first row of fasteners in the spar cap member. The actual failure is shown to have occurred at a lower load level than had been predicted, but this result is a least partially attributable to the difference in overall load sharing between joint members. While the analysis model predicted nearly equal load sharing between the wing skin and spar cap members, the test results (discussed earlier in Section 5) indicated that the spar cap member was working to about a 10-percent-higher stress level than the skin.

This slight difference between the analysis and test results may have occurred for several reasons. The analysis model did not include a detailed representation of the specimen end fittings, which could have affected the load sharing between the skin and spar. The load redistribution which may have resulted

from the specimen eccentricities and secondary effects may not have been reflected by the deformations of the model under load. Regardless of why this took place, the 8-percent variation between analysis and test results could have easily resulted from the effects of fastener hole tolerances, variations in material properties, etc.

Based on the tested strain level in the spar cap member, it appears that the bearing-bypass curve of Figure 47 was accurate. Had the analysis model reflected the "exact" strain level in the spar cap member as it occurred in the test, the strength prediction would have been equally "exact." In any case, the analyses conducted for each of the Phase II multirow joint tests did not include any conservative (or unconservative) assumptions, and the correlation achieved throughout the program was a successful demonstration of the analysis methodology.

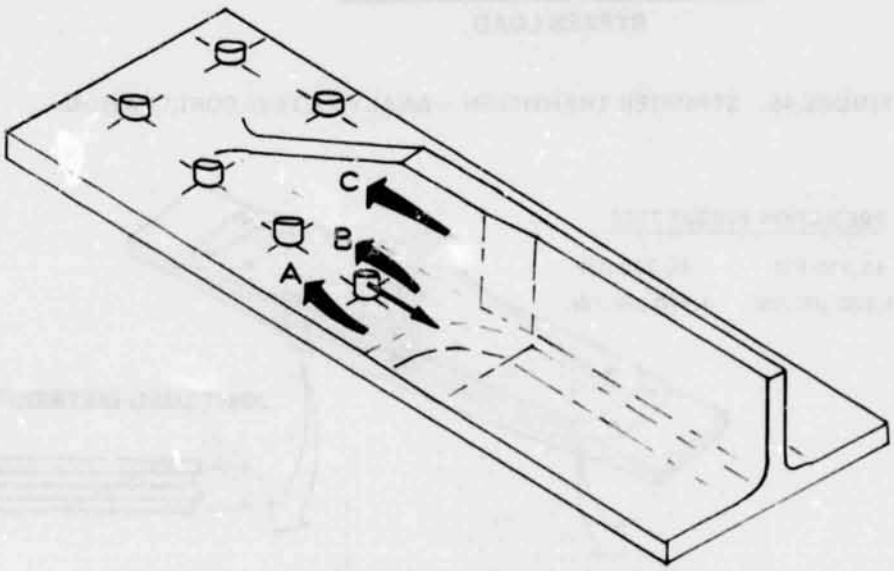

FIGURE 44. BEARING-BYPASS LOADS IN STRINGER TRANSITION JOINT

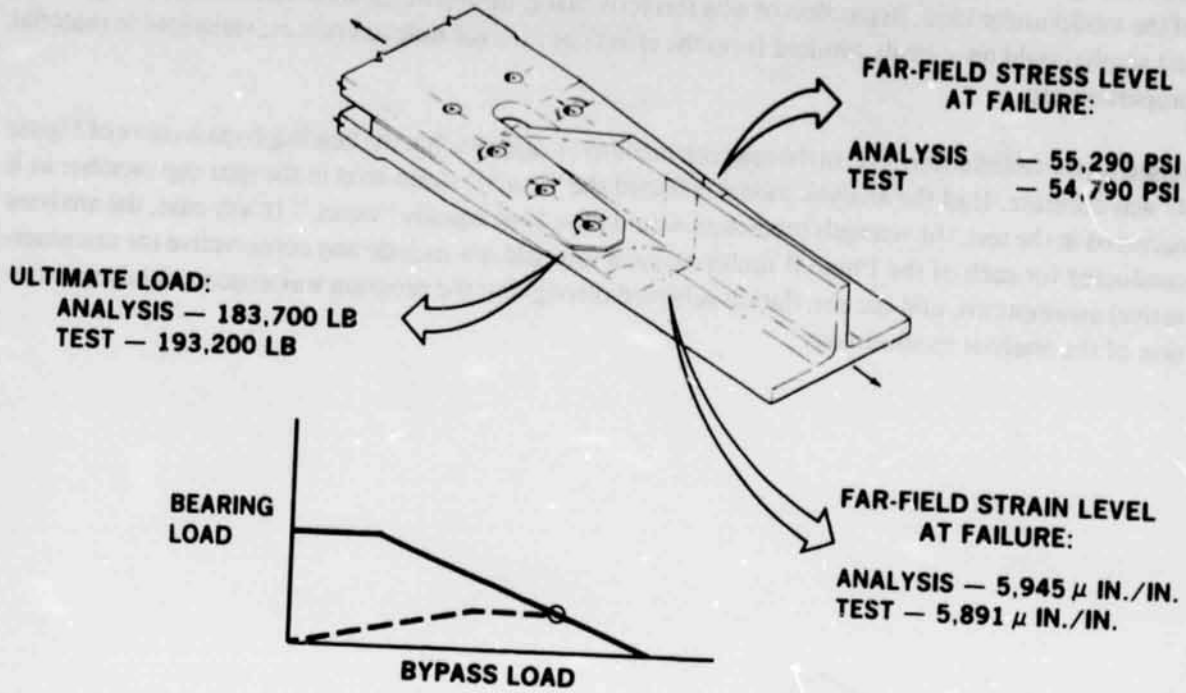

FIGURE 45. STRINGER TRANSITION – ANALYSIS/TEST CORRELATION

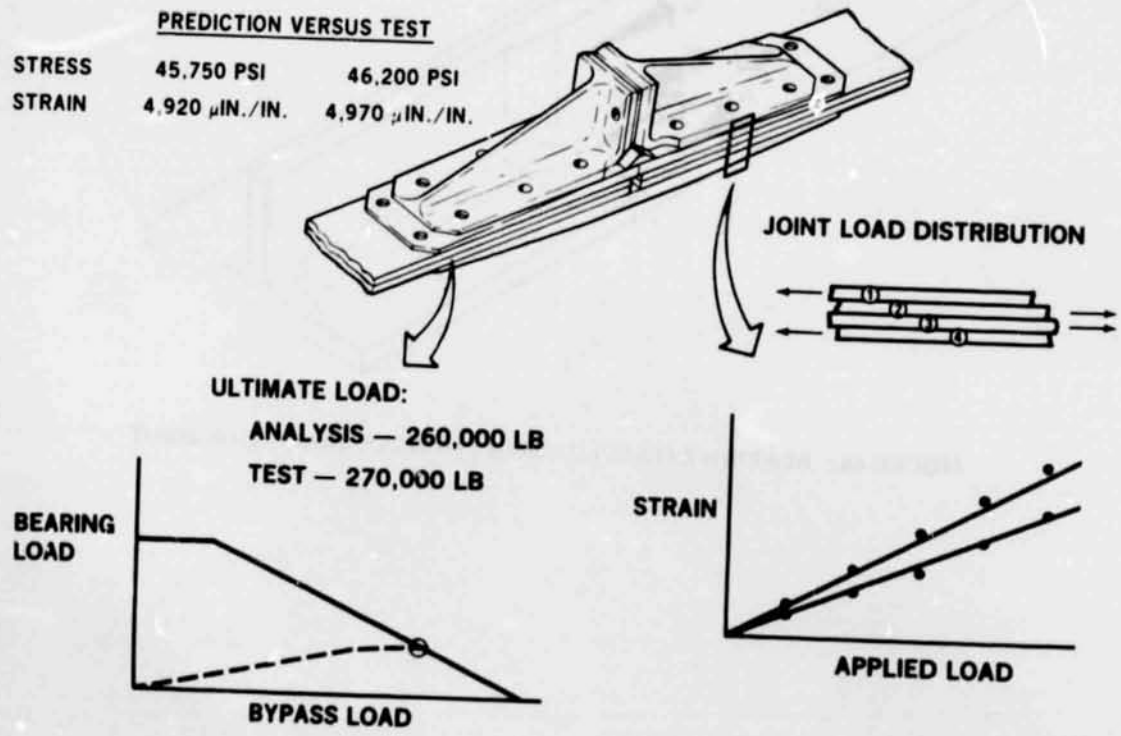

FIGURE 46. DEMONSTRATION SUBCOMPONENT – ANALYSIS/TEST CORRELATION

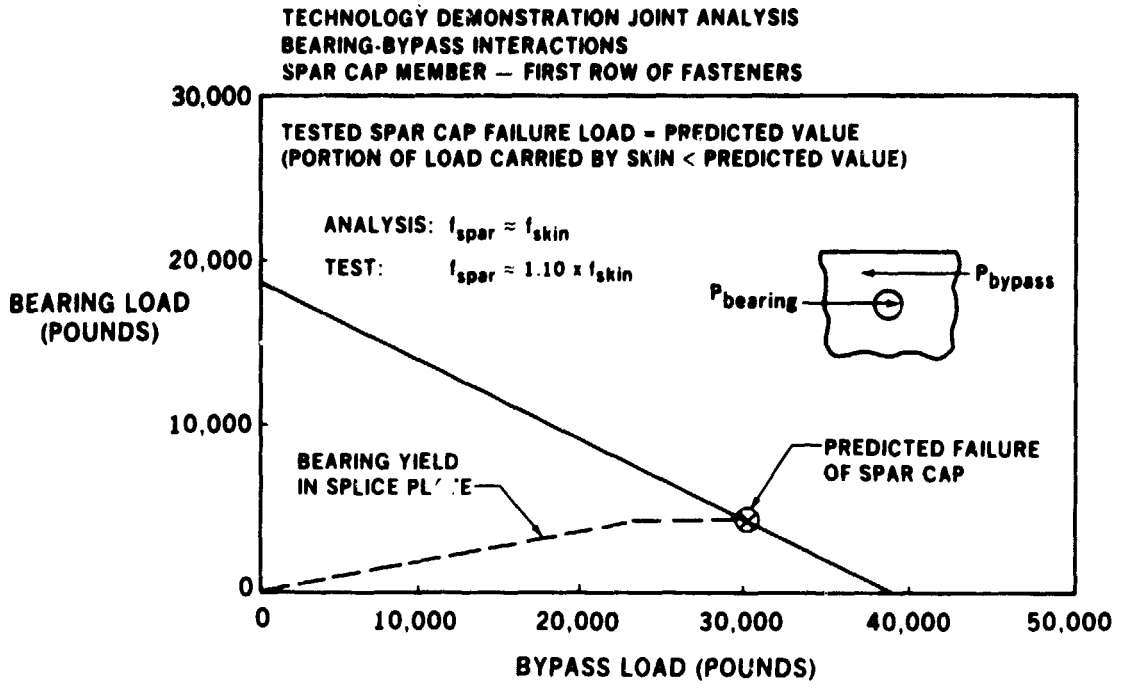

FIGURE 47. BEARING-BYPASS INTERACTIONS – TECHNOLOGY DEMONSTRATION TEST

SECTION 8
CONCLUSIONS

The results obtained in this program have demonstrated the ability to design and fabricate critical structural joints for large composite wing structure representative of a commercial transport aircraft. The analysis methods developed throughout the program were shown to give reliable strength predictions for large multirow bolted joints in fibrous composite laminates. Gross-section stress levels on the order of 45,000 to 50,000 psi and corresponding strain levels of 4,700 to 5,000 microstrain were achieved in most cases.

The key to maximizing the strength of bolted composite joints is in restricting the bearing stresses at the most critically loaded locations. For constant-thickness skins, the critical location for tension failures will typically be the outermost row of fasteners where the combination of bearing and bypass loads is the highest. The nature of bearing-bypass interactions in most composite laminates is such that the highest strength will be attained by minimizing the bearing load at the first row of bolts, and maximizing the bypass load which can then be transferred by the remaining fastener rows.

The most efficient joint designs have uniform-thickness skins in combination with tapered splice plates and tailored fastener sizes in order to achieve the desired bolt load distributions. The use of unreinforced skins also facilitates straightforward bolted repairs in areas away from the joint. Thickness buildups at bolted joints are permitted if warranted by the design, as long as the basic structure outside the joint is not so highly stressed as to make it unrepairable.

The strength of multirow bolted joints in composite structures is governed by the associated bearing-bypass load interaction under tensile or compressive loads. However, the potential for fastener failures either in shear or bending should not be overlooked. An accurate load-sharing analysis method, such as the A4EJ program, is required to perform accurate strength predictions, which can account for any nonlinear effects which may influence the bolt load distributions. For more complex joint structure, such solutions can be achieved through the use of finite element analyses in combination with semi-empirical methods.

The design of critical joints in highly loaded composite wing structure may often be the limiting factor in establishing ultimate design strain levels. Thus, the joint designs should be optimized first, before the "basic" structural concepts are selected, to ensure that the final configuration can withstand the design loads at each critical joint and to preserve the inherent repairability of the structure. This approach will avoid any compromises in the joint designs which would eventually result in a lower overall structural efficiency. For transport wing structure, any small extra weight in the splice plate material or fasteners is worth incurring in order to maximize the efficiency of the heavy skins. Metal materials are often the best choice for splice plate design, particularly where the potential exists for critical interlaminar or out-of-plane forces.

Not all joint geometries or load conditions were examined during this program, and a substantial body of work remains. The multirow compression joints tested during Phase I identified new failure modes which warrant further investigation. All of the joint tests discussed here were subjected to uniaxial loads. In actual structure, biaxial or triaxial stress states are often encountered, and efforts toward the development of methodology which can account for these effects must continue. Despite the relative complexity of the technology demonstration joint test, the performance or behavior of an actual wing box structure

is substantially more complex. Unexpected forces due to secondary effects can often arise which are difficult, if not impossible, to predict analytically. Only the successful testing of a representative wing box structure would provide a sufficient level of confidence in the selected joint design concepts.

The high gross-section strains exhibited by the bolted joints tested in this program indicate that highly loaded bolted joints in primary composite structures are feasible. However, the design, analysis, and manufacture of such structure require more attention to detail than for ductile metal alloys. The optimum designs and trends presented here are not all-inclusive, and the results of the parametric studies used to develop these trends will change with the evolution of more advanced and improved material systems.

SECTION 9
REFERENCES

1. Bunin, B. L. and Sagui, R. L., Critical Joints in Large Composite Primary Aircraft Structures, Volume III — Ancillary Data Test Results, NASA-CR-172588, 1985.

2. Bunin, B. L., Critical Composite Joint Subcomponents — Analysis and Test Results, NASA CR-3711, September 1983.

3. Hart-Smith, L. J., Bolted Joints in Graphite-Epoxy Composites, NASA CR-144899, January 1976.

4. Hart-Smith, L. J., Design Methodology for Bonded-Bolted Composite Joints, USAF Contract Report AFWAL-TR-81-3154, Vols.I and II, February 1982. (Available from DTIC as AD A117 342.)

5. Nelson, W. D., Bunin, B. L. and Hart-Smith, L. J., Critical Joints in Large Composite Aircraft Structure, NASA CR-3710, August 1983.

6. Garbo, S. P. and Ogonowski, J. M., Effect of Variance and Manufacturing Tolerances on the Design Strength and Life of Mechanically Fastened Composite Joints, USAF Contract Report AFWAL-TR-81-3041, Vols.I-IV, April 1981.

7. Hart-Smith, L. J., Mechanically Fastened Joints for Advanced Composites — Phenomenological Considerations and Simple Analyses, Douglas Aircraft Company Paper 6748A presented to the Fourth Conference on Fibrous Composites in Structural Design, San Diego, California, November 1978.

8. Tate, M. B. and Rosenfeld, S. J., Preliminary Investigation of the Loads Carried by Individual Bolts in Bolted Joints, NACA TN 1051, May 1946.

9. Bunin, B. L., Studies on Highly Loaded Bolted Joints in Composite Structures, Douglas Aircraft Company Paper 7418 presented to the 29th National SAMPE Symposium and Exhibition, Reno, Nevada, April 1984.

10. Bunin, B. L., Critical Joints in Large Composite Primary Aircraft Structures, Volume II — Technology Demonstration Test Report, NASA CR-172587, 1985.

1. Report No.	2. Government Accession No.	3. Recipient's Catalog No.
NASA CR-3914		

4. Title and Subtitle	5. Report Date
Critical Joints in Large Composite Primary Aircraft Structures Volume I - Technical Summary	September 1985
	6. Performing Organization Code
7. Author(s)	8. Performing Organization Report No.
B. L. Bunin	ACEE-26-FR-3504
	10. Work Unit No.
9. Performing Organization Name and Address	11. Contract or Grant No.
Douglas Aircraft Company 3855 Lakewood Blvd. Long Beach, Ca. 90845	NAS1-16857
	13. Type of Report and Period Covered
12. Sponsoring Agency Name and Address	Contractor Report
National Aeronautics & Space Administration Washington D.C., 20546	14. Sponsoring Agency Code
	534-03-13-30

15. Supplementary Notes

NASA Langley Technical Monitor: Andrew J. Chapman
FINAL REPORT

16. Abstract

A program was conducted at Douglas Aircraft Company to develop the technology for critical joints in composite wing structure that meets all the design requirements of a 1990 commercial transport aircraft. In fulfilling this objective, analytical procedures for joint design and analysis were developed during Phase I of the program. Tests were conducted at the element level to supply the empirical data required for methods development. Large composite multirow joints were tested to verify the selected design concepts and for correlation with analysis predictions. The Phase II program included additional tests to provide joint design and analysis data, and culminated with several technology demonstration tests of a major joint area representative of a commercial transport wing. After a review of the Phase I effort, this report focuses on the technology demonstration program of Phase II. The analysis methodology development, structural test program, and correlation between test results and analytical strength predictions are reviewed.

17. Key Words (Suggested by Author(s))	18. Distribution Statement
Advanced Composite Structures Bolted Joints Composite Wing Test Results	Subject Category 24

19. Security Classif. (of this report)	20. Security Classif. (of this page)	21. No. of Pages	22. Price
Unclassified	Unclassified	64	